

# NONPARAMETRIC TEACHING OF ATTENTION LEARNERS

000  
001  
002  
003  
004  
005  
006  
007  
008  
009  
010  
011  
012  
013  
014  
015  
016  
017  
018  
019  
020  
021  
022  
023  
024  
025  
026  
027  
028  
029  
030  
031  
032  
033  
034  
035  
036  
037  
038  
039  
040  
041  
042  
043  
044  
045  
046  
047  
048  
049  
050  
051  
052  
053  
Anonymous authors  
Paper under double-blind review

## ABSTRACT

Attention learners, neural networks built on the attention mechanism, *e.g.*, transformers, excel at learning the implicit relationships that relate sequences to their corresponding properties, *e.g.*, mapping a given sequence of tokens to the probability of the next token. However, the learning process tends to be costly. To address this, we present a novel paradigm named **Attention Neural Teaching** (AtteNT) that reinterprets the learning process through a nonparametric teaching perspective. Specifically, the latter provides a theoretical framework for teaching mappings that are implicitly defined (*i.e.*, nonparametric) via example selection. Such an implicit mapping is embodied through a dense set of sequence-property pairs, with the AtteNT teacher selecting a subset to accelerate convergence in attention learner training. By analytically investigating the role of attention on parameter-based gradient descent during training, and recasting the evolution of attention learners, shaped by parameter updates, through functional gradient descent in nonparametric teaching, we show *for the first time* that teaching attention learners is consistent with teaching importance-adaptive nonparametric learners. These new findings readily commit AtteNT to enhancing learning efficiency of attention learners. Specifically, we observe training time reductions of 13.01% for LLMs and 20.58% for ViTs, spanning both fine-tuning and training-from-scratch regimes. Crucially, these gains are achieved without compromising accuracy; in fact, performance is consistently preserved and often enhanced across a diverse set of downstream tasks.

## 1 INTRODUCTION

The attention mechanism, inspired by human attention concepts (Ahmad, 1991; Soydane, 2022), is designed to assess the relative importance of each element in a sequence (Bahdanau et al., 2015; Vaswani et al., 2017). By leveraging attention, neural networks can effectively learn the implicit relationships that map sequences to their corresponding properties, *e.g.*, mapping a sequence of tokens to the probability of the next token. These Attention Neural Networks (ANNs), *e.g.*, transformers (Vaswani et al., 2017; Kong et al., 2019), have achieved significant success in a wide range of downstream tasks across various fields, including natural language processing (Vaswani et al., 2017; Devlin et al., 2019; Consens et al., 2025), computer vision (Dosovitskiy et al., 2020; Azad et al., 2024; Chen et al., 2024), and multimodal systems (Nagrani et al., 2021; Yang et al., 2024).

However, the process of learning the implicit mappings—*i.e.*, training—can be quite costly for ANNs, especially when handling large-scale tasks (Liu et al., 2018b; Beltagy et al., 2019; Gu et al., 2021; Yang et al., 2023). For instance, pretraining language models often requires training on corpora with millions of sentences (Common Crawl, 2007; Li et al., 2024). In the case of video understanding, the scale can become overwhelmingly large (Bain et al., 2021; Sharma et al., 2018; Shu et al., 2025). As a result, reducing training costs and enhancing learning efficiency has become an urgent priority.

Recent research on nonparametric teaching (Zhang et al., 2023b;a; 2024a; 2025) presents a promising solution to the issue outlined above. Specifically, nonparametric teaching provides a theoretical framework for selecting examples efficiently when the target mapping (*i.e.*, either a function or a model) being taught is nonparametric, *i.e.*, implicitly defined. It builds on the concept of machine teaching (Zhu, 2015; Zhu et al., 2018), which involves designing a training set (dubbed the teaching set) to help the learner quickly converge to the target functions, while relaxing the assumption that the target functions are parametric (Liu et al., 2017; 2018a), thus enabling the teaching of nonparametric

(non-closed-form) functions with a focus on function space. Unfortunately, these studies are limited to multilayer perceptron-based learners and do not account for the attention mechanism, making their direct application difficult when the learners are ANNs. Additionally, ANNs are typically updated through gradient descent in parameter space, which contrasts with the functional gradient descent used in nonparametric teaching within function space (Zhang et al., 2023b;a; 2024a; 2025). Hence, it is not immediate to apply nonparametric teaching theory to attention learners.

To this end, we systematically investigate the role of attention on ANN gradient-based training in both parameter and function spaces. Specifically, we analytically examine how attention adaptively assigns different importance to each element in an input sequence during parameter-based gradient descent in parameter space, and explicitly show that the parameter gradient retains the same form as the input sequence size scales. This importance-adaptive update in parameter space drives the evolution of the ANN, which can be expressed using the dynamic Attention Neural Tangent Kernel (ANTK) (Yang, 2019; Hron et al., 2020), and then cast into function space. We prove that this dynamic ANTK converges to the importance-adaptive canonical kernel used in functional gradient descent, suggesting that the evolution of ANN under parameter gradient descent is consistent with that under functional gradient descent. Therefore, it is natural to interpret the learning process of attention learners through the theoretical framework of nonparametric teaching: the target mapping is represented by a dense set of sequence-property pairs, where each sequence is associated with its target output, and the teacher selects a subset of these pairs to provide to the ANN, ensuring rapid convergence of this attention learner. Consequently, to improve the learning efficiency of ANNs, we propose a novel paradigm called AtteNT, where the teacher applies a counterpart of the greedy teaching algorithm from nonparametric teaching to train attention learner, specifically by selecting the sequence with the greatest discrepancy between their true property values and the ANN outputs. Lastly, we carry out comprehensive experiments to demonstrate the effectiveness of AtteNT across various scenarios, including both natural language processing and computer vision tasks. Our key contributions are as follows:

- We propose AtteNT, a novel paradigm that interprets attention learner training through the theoretical lens of nonparametric teaching. This facilitates the use of greedy algorithms from nonparametric teaching to effectively improve the learning efficiency of attention learners.
- We analytically investigate the role of attention in parameter-based gradient descent within parameter space, revealing the consistency between the evolution of ANN driven by parameter updates and that under functional gradient descent in nonparametric teaching. We further show that the dynamic ANTK, emerging from gradient descent on the parameters, converges to the importance-adaptive canonical kernel of functional gradient descent. These findings bridge nonparametric teaching theory with attention learner training, thereby broadening the application of nonparametric teaching to contexts involving attention mechanisms.
- We demonstrate the effectiveness of AtteNT through extensive experiments across both natural language processing (NLP) and computer vision (CV) tasks. Our approach reduces Large Language Model (LLM) fine-tuning time by 13.01% and accelerates Vision Transformer (ViT) training from scratch by 20.58%, thereby providing strong empirical support for our theoretical claims.

## 2 RELATED WORKS

**Attention learners.** The effectiveness of the attention mechanism in learning implicit mappings from sequences to relevant properties has spurred a surge in research on attention learners (Bahdanau et al., 2015; Vaswani et al., 2017; Kong et al., 2019). This growing interest is particularly evident in the increasing efforts to apply attention learners across a wide variety of downstream tasks, including natural language processing (Galassi et al., 2020; Jin et al., 2024), computer vision (Dosovitskiy et al., 2020; Hassanin et al., 2024; Zhang et al., 2024b), medicine (Thirunavukarasu et al., 2023; Demszky et al., 2023), and graph-related fields (Veličković et al., 2018; Wu et al., 2024). Various efforts have been made in designing learners for improved mapping learning in vision tasks (Lin et al., 2022; Dosovitskiy et al., 2020; Arnab et al., 2021), as well as for more efficient inference (Kitaev et al., 2020; Katharopoulos et al., 2020; Lu et al., 2021). There have also been ongoing pursuits to enhance learning efficiency, such as sparse training (Frankle & Carbin, 2018; You et al., 2020; Chen et al., 2021c;b; Li et al., 2023), improved initialization (Huang et al., 2020; d’Ascoli et al., 2021), and data curation (Tang et al., 2023; Zhong et al., 2023; Lin et al., 2024; Li et al., 2024). Differently, we frame

108 attention learner training from a fresh perspective of nonparametric teaching (Zhang et al., 2023b;a),  
 109 and adopt a corresponding variant of the greedy algorithm to enhance the training efficiency of ANNs.  
 110

111 **Nonparametric teaching.** Machine teaching (Zhu, 2015; Zhu et al., 2018) focuses on designing a  
 112 teaching set that allows the learner to quickly converge to a target model function. It can be seen  
 113 as the reverse of machine learning: while machine learning aims to learn a mapping from a given  
 114 training set, machine teaching seeks to construct the set based on a desired mapping. Its effectiveness  
 115 has been demonstrated across various domains, including crowdsourcing (Singla et al., 2014; Zhou  
 116 et al., 2018), robustness (Alfeld et al., 2017; Ma et al., 2019; Rakhsha et al., 2020), and computer  
 117 vision (Wang et al., 2021a; Wang & Vasconcelos, 2021). Nonparametric teaching (Zhang et al.,  
 118 2023b;a) extends iterative machine teaching (Liu et al., 2017; 2018a) by broadening the parameterized  
 119 family of target mappings to encompass the more general nonparametric framework. This theoretical  
 120 framework has proven effective in enhancing the efficiency of multilayer perceptrons for learning  
 121 implicit functions from signal coordinates to corresponding values (Zhang et al., 2024a; Luo et al.,  
 122 2024), as well as improving the training efficiency of graph convolutional networks for learning  
 123 implicit mappings from graphs to their relevant properties (Zhang et al., 2025). Nevertheless, the  
 124 absence of the attention mechanism in these studies limits their direct applicability to general tasks  
 125 involving attention learners (Bahdanau et al., 2015; Vaswani et al., 2017). This work systematically  
 126 investigates the role of attention and highlights the alignment between the evolution of ANN driven by  
 127 parameter updates and that guided by functional gradient descent in nonparametric teaching. These  
 128 insights, for the first time, broaden the scope of nonparametric teaching in attention learner training,  
 129 positioning our AtteNT as a novel approach to improving ANN learning efficiency.  
 130

### 3 BACKGROUND

131 **Notation.**<sup>1</sup> Let  $(\mathbf{x}_1, \dots, \mathbf{x}_S)$  represent a sequence of length  $S$ , where each  $\mathbf{x}_s \in \mathbb{R}^d$  denotes a  
 132  $d$ -dimensional feature vector associated with the  $s$ -th element, with  $s \in \mathbb{N}_S$  ( $\mathbb{N}_S := \{1, \dots, S\}$ ).  
 133 Each  $\mathbf{x}_s$  is a row vector, expressed as  $[\mathbf{x}_{s,j}]_d^\top = [x_{s,1}, \dots, x_{s,d}]$ . The entire collection of feature  
 134 vectors forms an  $S \times d$  feature matrix, denoted  $\mathbf{S}_{S \times d} \in \mathcal{S} \subseteq \mathbb{R}^{S \times d}$  (or simply  $\mathcal{S}$ ). The  $s$ -th row and  
 135 the  $i$ -th column of this matrix, corresponding to the  $s$ -th element and the  $i$ -th feature, are denoted  
 136 by  $\mathbf{S}_{(s,:)}$  and  $\mathbf{S}_{(:,i)}$ , respectively. Alternatively, these can be written as  $\mathbf{e}_s^\top \mathbf{S}$  and  $\mathbf{S} \mathbf{e}_i$ , where  $\mathbf{e}_i$  is  
 137 a standard basis vector with its  $i$ -th entry being 1 and all other entries equal to 0. The bold column  
 138 vector  $\mathbf{1}$  represents a vector in which all elements are 1. The property of the sequence is represented  
 139 by  $\mathbf{y} \in \mathcal{Y}$ , where  $\mathbf{y}$  is a scalar for sequence-level properties ( $\mathcal{Y} \subseteq \mathbb{R}$ ) and a vector for element-level  
 140 properties ( $\mathcal{Y} \subseteq \mathbb{R}^n$ ). A set with  $m$  items is denoted as  $\{a_i\}_m$ . If  $\{a_i\}_m \subseteq \{a_i\}_n$ , then  $\{a_i\}_m$   
 141 represents a subset of  $\{a_i\}_n$  containing  $m$  items, where the indices are  $i \in \mathbb{N}_n$ . A diagonal matrix  
 142 with diagonal entries  $a_1, \dots, a_m$  is denoted as  $\text{diag}(a_1, \dots, a_m)$ , and if all  $m$  values are identical,  
 143 the matrix is simplified as  $\text{diag}(a; m)$ .

144 Let  $K(\mathbf{S}, \mathbf{S}') : \mathcal{S} \times \mathcal{S} \mapsto \mathbb{R}$  denote a symmetric and positive definite sequence kernel (Canc-  
 145 cedda et al., 2003; Király & Oberhauser, 2019). This kernel can also be expressed as  $K(\mathbf{S}, \mathbf{S}') = K_{\mathbf{S}}(\mathbf{S}') = K_{\mathbf{S}'}(\mathbf{S})$ , where for simplicity,  $K_{\mathbf{S}}(\cdot)$  may be abbreviated as  $K_{\mathbf{S}}$ . The reproducing  
 146 kernel Hilbert space (RKHS)  $\mathcal{H}$  associated with  $K(\mathbf{S}, \mathbf{S}')$  is defined as the closure of the linear  
 147 span  $\{f : f(\cdot) = \sum_{i=1}^r a_i K(\mathbf{S}_i, \cdot), a_i \in \mathbb{R}, r \in \mathbb{N}, \mathbf{S}_i \in \mathcal{S}\}$ , with the inner product given by  
 148  $\langle f, g \rangle_{\mathcal{H}} = \sum_{ij} a_i b_j K(\mathbf{S}_i, \mathbf{S}_j)$ , where  $g = \sum_j b_j K_{\mathbf{S}_j}$  (Liu & Wang, 2016; Zhang et al., 2023b).  
 149 Rather than assuming the idealized case of a closed-form solution  $f^*$ , we focus on the more realistic  
 150 scenario where the realization of  $f^*$  is given (Zhang et al., 2023b;a; 2024a; 2025). Given the target  
 151 mapping  $f^* : \mathcal{S} \mapsto \mathcal{Y}$ , it uniquely maps each sequence  $\mathbf{S}_\dagger$  to its corresponding output  $\mathbf{y}_\dagger$ , such that  
 152  $\mathbf{y}_\dagger = f^*(\mathbf{S}_\dagger)$ . According to the Riesz–Fréchet representation theorem (Lax, 2014; Schölkopf &  
 153 Smola, 2002; Zhang et al., 2023b), the evaluation functional is defined as follows:  
 154

155 **Definition 1.** Let  $\mathcal{H}$  denote a reproducing kernel Hilbert space<sup>2</sup> equipped with a positive definite  
 156 sequence kernel  $K_{\mathbf{S}} \in \mathcal{H}$ , where  $\mathbf{S} \in \mathcal{S}$ . The evaluation functional  $E_{\mathbf{S}}(\cdot) : \mathcal{H} \mapsto \mathbb{R}$  is defined by the  
 157 reproducing property as

$$E_{\mathbf{S}}(f) = \langle f, K_{\mathbf{S}}(\cdot) \rangle_{\mathcal{H}} = f(\mathbf{S}), \quad f \in \mathcal{H}. \quad (1)$$

160 <sup>1</sup>The notation table can be found in Appendix A.1.

161 <sup>2</sup>In nonparametric teaching, the extension from scalar-valued to vector-valued functions, relating to element-  
 162 level properties, is a well-established generalization in Zhang et al., 2023a.

Furthermore, for a functional  $F : \mathcal{H} \mapsto \mathbb{R}$ , the Fréchet derivative (Coleman, 2012; Liu, 2017; Zhang et al., 2023b) of  $F$  is defined as:

**Definition 2.** (Fréchet derivative in RKHS) The Fréchet derivative of a functional  $F : \mathcal{H} \mapsto \mathbb{R}$  at a point  $f \in \mathcal{H}$ , represented as  $\nabla_f F(f)$ , is defined implicitly by  $F(f + \epsilon g) = F(f) + \langle \nabla_f F(f), \epsilon g \rangle_{\mathcal{H}} + o(\epsilon)$  for any  $g \in \mathcal{H}$  and  $\epsilon \in \mathbb{R}$ . This derivative itself is a function in  $\mathcal{H}$ .

**Attention learners**, referring to neural networks that incorporate attention mechanisms, are designed to learn the implicit mapping between input sequences and their associated properties (Vaswani et al., 2017). Specifically, the attention consists of three components: the query matrix  $\mathcal{Q}(\mathbf{S}) := \mathbf{S}\mathbf{W}^Q$ , the key matrix  $\mathcal{K}(\mathbf{S}) := \mathbf{S}\mathbf{W}^K$ , and the value matrix  $\mathcal{V}(\mathbf{S}) := \mathbf{S}\mathbf{W}^V$ , where the query and key weight matrices  $\mathbf{W}^Q$  and  $\mathbf{W}^K$  are of size  $d \times p$ , and the value weight matrix  $\mathbf{W}^V$  is of size  $d \times v$ . For simplicity, this paper primarily focuses on a single-layer, single-head self-attention neural network<sup>3</sup> (Mahankali et al., 2024; Makkuvu et al., 2025), which can be expressed as

$$f_{\theta}(\mathbf{S}) = \text{softmax} \left( \frac{\mathcal{Q}(\mathbf{S})\mathcal{K}(\mathbf{S})^{\top}}{\sqrt{d}} \right) \mathcal{V}(\mathbf{S}), \quad (2)$$

where  $\text{softmax}(\cdot)$  is applied row-wise.

**Nonparametric teaching** is formulated as a functional minimization over a teaching set, denoted as  $\mathcal{D} = \{(\mathbf{x}^1, y^1), \dots, (\mathbf{x}^T, y^T)\}$ , where each input  $\mathbf{x} \in \mathbb{R}^d$  represents independent feature vectors, without considering the sequence (Zhang et al., 2023b). The collection of all possible teaching sets is represented by  $\mathbb{D}$ :

$$\mathcal{D}^* = \arg \min_{\mathcal{D} \in \mathbb{D}} \mathcal{M}(\hat{f}, f^*) + \lambda \cdot \text{card}(\mathcal{D}) \quad \text{s.t.} \quad \hat{f} = \mathcal{A}(\mathcal{D}). \quad (3)$$

This formulation involves three key components:  $\mathcal{M}$  which measures the discrepancy between  $\hat{f}$  and  $f^*$  (e.g.,  $L_2$  distance in RKHS  $\mathcal{M}(\hat{f}^*, f^*) = \|\hat{f}^* - f^*\|_{\mathcal{H}}$ );  $\text{card}(\cdot)$ , representing the cardinality (or size) of the teaching set  $\mathcal{D}$ , controlled by a regularization constant  $\lambda > 0$ ; and  $\mathcal{A}(\mathcal{D})$ , which denotes the learning algorithm employed by the learners, typically based on empirical risk minimization:

$$\hat{f} = \arg \min_{f \in \mathcal{H}} \mathbb{E}_{\mathbf{x} \sim \mathbb{P}(\mathbf{x})} (\mathcal{L}(f(\mathbf{x}), f^*(\mathbf{x}))) \quad (4)$$

with a convex loss  $\mathcal{L}$  (w.r.t.  $f$ ), which is optimized using functional gradient descent:<sup>4</sup>

$$f^{t+1} \leftarrow f^t - \eta \underbrace{E_{\mathbf{x}} \left( \frac{\partial \mathcal{L}(f^*, f^t)}{\partial f^t} \right)}_{:= \mathcal{G}(\mathcal{L}, f^*; f^t, \mathbf{x}), \text{ Functional Gradient}} \cdot K_{\mathbf{x}}, \quad (5)$$

where  $t = 0, 1, \dots, T$  is the iteration index,  $\eta > 0$  is the learning rate, and  $E_{\mathbf{x}}(f) = f(\mathbf{x})$  denotes the evaluation functional.

## 4 ATTENT

We begin by investigating the role of attention in parameter-based gradient descent. Then, by translating the evolution of an ANN—driven by importance-adaptive updates in parameter space—into function space, we show that the evolution of the ANN under parameter gradient descent is consistent with that under functional gradient descent. Lastly, we present the greedy AttENT algorithm, which effectively selects sequences with steeper gradients to enhance the learning efficiency of the ANN.

### 4.1 IMPORTANCE-ADAPTIVE UPDATE IN THE PARAMETER SPACE

<sup>3</sup>This can be directly extended to other attention learners, including those with multi-head attention or different types of attention mechanisms (Dong et al., 2021; Kajitsuka & Sato, 2024).

<sup>4</sup>The functional gradient is obtained by applying the functional chain rule (Lemma 5) and the gradient of an evaluation functional (Lemma 6), both of which are detailed in Appendix A.2.

Let the column vector  $\theta \in \mathbb{R}^m$  denote all trainable weights in a flattened format, with  $m$  representing the total number of parameters in the ANN. Figure 1 illustrates the workflow of the ANN. Given a training set of size  $N$ ,  $\{(\mathbf{S}_i, \mathbf{y}_i) | \mathbf{S}_i \in \mathcal{S}, \mathbf{y}_i \in \mathcal{Y}\}_N$ , the parameters are updated via gradient descent, as shown below:<sup>5</sup>

$$\theta^{t+1} \leftarrow \theta^t - \frac{\eta}{NS} \sum_{i=1}^N \sum_{j=1}^S \nabla_{\theta} \mathcal{L}(f_{\theta^t}(\mathbf{S}_i)_{(j,:)}, \mathbf{y}_{i(j,:)})$$

where  $f_{\theta^t}(\mathbf{S}_i)_{(j,:)}$  refers to the  $j$ -th row of the output  $f_{\theta^t}(\mathbf{S}_i)$ , corresponding to the  $j$ -th element of the input sequence, and  $\mathbf{y}_{i(j,:)}$  denotes its associated property value. Since the learning rate  $\eta$  is small enough, the updates remain minimal over multiple iterations, allowing them to be treated as a time derivative and thus expressed as a differential equation (Jacot et al., 2018; Yang, 2019; Hron et al., 2020):

$$\frac{\partial \theta^t}{\partial t} = -\frac{\eta}{NS} \left[ \frac{\partial \mathcal{L}(f_{\theta^t}(\mathbf{S}_1), \mathbf{y}_1)}{\partial f_{\theta^t}(\mathbf{S}_1)}, \dots, \frac{\partial \mathcal{L}(f_{\theta^t}(\mathbf{S}_N), \mathbf{y}_N)}{\partial f_{\theta^t}(\mathbf{S}_N)} \right] \cdot \left[ \frac{\partial f_{\theta^t}(\mathbf{S}_i)}{\partial \theta^t} \right]_N. \quad (7)$$

The term  $\frac{\partial f_{\theta}(\mathbf{S})}{\partial \theta}$  (with the indexes  $i$  and  $t$  omitted for simplicity), which defines the direction for parameter updates, can be more explicitly written as

$$\frac{\partial f_{\theta}(\mathbf{S})}{\partial \theta} = \left[ \underbrace{\frac{\partial f_{\theta}(\mathbf{S})}{\partial \mathbf{W}^V_{(:,1)}}, \dots, \frac{\partial f_{\theta}(\mathbf{S})}{\partial \mathbf{W}^V_{(:,v)}}}_{\text{w.r.t. the value weight matrix}}, \underbrace{\frac{\partial f_{\theta}(\mathbf{S})}{\partial \mathbf{W}^Q_{(:,1)}}, \dots, \frac{\partial f_{\theta}(\mathbf{S})}{\partial \mathbf{W}^Q_{(:,p)}}}_{\text{w.r.t. the query weight matrix}}, \underbrace{\frac{\partial f_{\theta}(\mathbf{S})}{\partial \mathbf{W}^K_{(:,1)}}, \dots, \frac{\partial f_{\theta}(\mathbf{S})}{\partial \mathbf{W}^K_{(:,p)}}}_{\text{w.r.t. the key weight matrix}} \right]. \quad (8)$$

Here, each term represents the derivative of the output  $f_{\theta}(\mathbf{S})$  w.r.t. the weight column vectors. Unlike derivatives for multilayer perceptron-based learners, where the input is used only once, *i.e.*, the derivative depends on a single use of the input, the attention mechanism invokes the input three times at  $\mathcal{Q}$ ,  $\mathcal{K}$ , and  $\mathcal{V}$  separately, as depicted in Figure 1. To clearly demonstrate, in an analytical and explicit manner, how these three invocations allow attention to adaptively assign varying different importance to each element in an input sequence within parameter space, we present an example involving the derivative of an ANN with  $v = 1$ , meaning that each component of the output  $f_{\theta^t}(\mathbf{S})_{(j,:)}$  is a scalar:

$$\frac{\partial f_{\theta}(\mathbf{S})}{\partial \theta} = \left[ \frac{\partial f_{\theta}(\mathbf{S})}{\partial \mathbf{W}^V}, \frac{\partial f_{\theta}(\mathbf{S})}{\partial \mathbf{W}^Q_{(:,1)}}, \dots, \frac{\partial f_{\theta}(\mathbf{S})}{\partial \mathbf{W}^Q_{(:,p)}}, \frac{\partial f_{\theta}(\mathbf{S})}{\partial \mathbf{W}^K_{(:,1)}}, \dots, \frac{\partial f_{\theta}(\mathbf{S})}{\partial \mathbf{W}^K_{(:,p)}} \right], \quad (9)$$

where the term  $\frac{\partial f_{\theta}(\mathbf{S})}{\partial \mathbf{W}^V}$  has a shape of  $S \times d$ , and is given by

$$\frac{\partial f_{\theta}(\mathbf{S})}{\partial \mathbf{W}^V} = \left[ \frac{\exp(\mathcal{Q}_{(i,:)} \mathcal{K}^{\top} / \sqrt{d})}{\mathbf{1}^{\top} \exp(\mathcal{Q}_{(i,:)} \mathcal{K}^{\top} / \sqrt{d})} \right]_S \mathbf{S}, \quad (10)$$

where  $\exp(\cdot)$  denotes the element-wise exponential operator. For simplicity, we omit the arguments of  $\mathcal{Q}$ ,  $\mathcal{K}$ ,  $\mathcal{V}$ . For  $i \in \mathbb{N}_p$ , the term  $\frac{\partial f_{\theta}(\mathbf{S})}{\partial \mathbf{W}^Q_{(:,i)}}$  and  $\frac{\partial f_{\theta}(\mathbf{S})}{\partial \mathbf{W}^K_{(:,i)}}$  are

$$\frac{\partial f_{\theta}(\mathbf{S})}{\partial \mathbf{W}^Q_{(:,i)}} = \left[ d^{-1/2} \underbrace{\mathbf{S}_{(j,:)} \cdot \left( \underbrace{\mathcal{K}_{(:,i)}^{\top} \text{diag}(\text{softmax}(\mathcal{Q}_{(j,:}) \mathcal{K}_{(:,i)}^{\top} / \sqrt{d}))}_{1 \times S} \right)^{S \times 1} \underbrace{\mathcal{V} - \mathcal{K}_{(:,i)}^{\top} \left( \text{softmax}(\mathcal{Q}_{(j,:}) \mathcal{K}_{(:,i)}^{\top} / \sqrt{d})^{\top} \text{softmax}(\mathcal{Q}_{(j,:}) \mathcal{K}_{(:,i)}^{\top} / \sqrt{d}) \right)^{S \times S} \mathcal{V}}_{S \times 1} \right]_{S \times d}, \quad (11)$$

<sup>5</sup>Training sequences generally have the same length, corresponding to the maximum length, which is ensured by padding or truncating (Yu et al., 2023b; Ding et al., 2024). Therefore, this paper focuses on sequences of the same length unless noted otherwise. Results for varying lengths can be directly obtained.

$$\frac{\partial f_\theta(\mathcal{S})}{\partial \mathbf{W}_{(:,i)}^K} = \left[ d^{-1/2} \underbrace{\mathbf{S}_{(j,:)} \cdot \left( \underbrace{\mathcal{Q}_{(:,i)}^\top \text{diag}(\text{softmax}(\mathcal{Q}_{(j,i)} \mathcal{K}_{(:,i)}^\top / \sqrt{d})) \mathcal{V}^S}_{1 \times S} \right)}_{1 \times d} \right]_{S \times 1} - \underbrace{\mathcal{Q}_{(:,i)}^\top \left( \text{softmax}(\mathcal{Q}_{(j,i)} \mathcal{K}_{(:,i)}^\top / \sqrt{d}) \right)^\top \text{softmax}(\mathcal{Q}_{(j,i)} \mathcal{K}_{(:,i)}^\top / \sqrt{d}) \underbrace{\mathcal{V}^S}_{S \times 1} \right]_{S \times d}. \quad (12)$$

The derivation is provided in Appendix A.3. For the sake of brevity, we focus on the query gradient, with similar results holding for the key and value gradients. As a result of invoking the input three times, Equation 11 reveals that the ANN gradient depends not only on the features of the sequence elements, *i.e.*,  $\mathbf{S}_{(j,:)}$ , but also on a scalar  $\omega_j$  that is specific to each element.

Specifically, Equation 11 explicitly shows that the gradient row order follows the order of elements in the input sequence, meaning the gradient is equivariant w.r.t. reordering the elements. This is in contrast to the gradient in recurrent neural networks (Elman, 1990; Jordan, 1997), where the order of the elements determines the power of the recurrent weights. Moreover, this gradient property is derived during the training stage, yet, interestingly, it aligns with the permutation invariance property of self-attention during inference (Lee et al., 2019).

The scalar  $\omega_j$  in Equation 11 is computed from  $\mathcal{Q}$ ,  $\mathcal{K}$ , and  $\mathcal{V}$ , which reflects the three invocations of input by the attention. It is clear that it is closely associated with the  $j$ -th element, meaning it is element-specific. This scalar is the importance value that attention assigns to each element, leading to an importance-adaptive update in the parameter space. When all importance values are set to 1, the gradient of the ANN reduces to the derivative of a multilayer perceptron without nonlinear activations and with batch input. Additionally, the explicit expressions in Equations 7, 11, and 12 show that the ANN gradient does not depend on the input sequence length (*i.e.*, the number of elements), as this is averaged out. Instead, it depends on the feature dimension. In other words, the parameter gradient remains unchanged even if the input sequence length  $S$  is scaled.

## 4.2 THE FUNCTIONAL EVOLUTION OF ANN

The importance-adaptive update in the parameter space drives the functional evolution of  $f_\theta \in \mathcal{H}$ . This variation in  $f_\theta$ , reflecting how  $f_\theta$  responds to updates in  $\theta$ , can be derived using Taylor's theorem as follows:

$$f(\theta^{t+1}) - f(\theta^t) = \langle \nabla_\theta f(\theta^t), \theta^{t+1} - \theta^t \rangle + o(\theta^{t+1} - \theta^t), \quad (13)$$

where  $f(\theta^\dagger) \equiv f_{\theta^\dagger}$ . In a manner analogous to the transformation of parameter updates into their differential form, this can also be expressed in a differential form (Zhang et al., 2024a):

$$\frac{\partial f_{\theta^t}}{\partial t} = \underbrace{\left\langle \frac{\partial f(\theta^t)}{\partial \theta^t}, \frac{\partial \theta^t}{\partial t} \right\rangle}_{(*)} + o\left(\frac{\partial \theta^t}{\partial t}\right). \quad (14)$$

By substituting the specific parameter updates, *i.e.*, Equation 7, into the first-order approximation term  $(*)$  of this variation, we obtain

$$\frac{\partial f_{\theta^t}}{\partial t} = -\frac{\eta}{NS} \left[ \frac{\partial \mathcal{L}(f_{\theta^t}(\mathcal{S}_1), \mathcal{y}_1)}{\partial f_{\theta^t}(\mathcal{S}_1)}, \dots, \frac{\partial \mathcal{L}(f_{\theta^t}(\mathcal{S}_N), \mathcal{y}_N)}{\partial f_{\theta^t}(\mathcal{S}_N)} \right] \cdot [K_{\theta^t}(\mathcal{S}_i, \cdot)]_N + o\left(\frac{\partial \theta^t}{\partial t}\right), \quad (15)$$

where the symmetric and positive definite  $K_{\theta^t}(\mathcal{S}_i, \cdot) := \left\langle \frac{\partial f_{\theta^t}(\mathcal{S}_i)}{\partial \theta^t}, \frac{\partial f_{\theta^t}(\cdot)}{\partial \theta^t} \right\rangle$  (for detailed derivations and further discussion, see Appendix A.4). Due to the inclusion of nonlinear activation functions in  $f(\theta)$ , the nonlinearity of  $f(\theta)$  with respect to  $\theta$  results in the remainder  $o(\theta^{t+1} - \theta^t)$  being nonzero. In a subtle difference, Jacot et al., 2018; Yang, 2019; Hron et al., 2020 apply the chain rule directly, giving less focus to the convexity of  $\mathcal{L}$  with respect to  $\theta$ . As a result, the first-order approximation is derived as the variation, with  $K_\theta$  being referred to as the Attention Neural Tangent Kernel (ANTK). It has been demonstrated that the ANTK remains constant during training when the ANN width, *i.e.*,  $d$ , is assumed to be infinite (Hron et al., 2020). However, in practical applications, the ANN width does not need to be infinitely large, prompting us to explore the dynamic ANTK (an example of how the ANTK is computed can be found in Figure 3 in Appendix A.4).

Consider characterizing the variation of  $f_\theta \in \mathcal{H}$  from a high-level, functional viewpoint (Zhang et al., 2024a; 2025). Using functional gradient descent, it can be written as

$$\frac{\partial f_{\theta^t}}{\partial t} = -\eta \mathcal{G}(\mathcal{L}, f^*; f_{\theta^t}, \{\mathcal{S}_i\}_N), \quad (16)$$

324 where the functional gradient is expressed as  
 325

$$326 \quad \mathcal{G}(\mathcal{L}, f^*; f_{\theta^t}, \{\mathbf{S}_i\}_N) = \frac{1}{NS} \left[ \frac{\partial \mathcal{L}(f_{\theta^t}(\mathbf{S}_1), \mathbf{y}_1)}{\partial f_{\theta^t}(\mathbf{S}_1)}, \dots, \frac{\partial \mathcal{L}(f_{\theta^t}(\mathbf{S}_N), \mathbf{y}_N)}{\partial f_{\theta^t}(\mathbf{S}_N)} \right] [K(\mathbf{S}_i, \cdot)]_N. \quad (17)$$

328 The asymptotic relationship between ANTK and the importance-adaptive canonical kernel (Cancedda  
 329 et al., 2003; Király & Oberhauser, 2019; Zhang et al., 2024a) in the context of functional gradient is  
 330 presented in Theorem 3 below, with the proof provided in Appendix B.1.

331 **Theorem 3.** *Given a convex loss  $\mathcal{L}$  and a training set  $\{(\mathbf{S}_i, \mathbf{y}_i) | \mathbf{S}_i \in \mathcal{S}, \mathbf{y}_i \in \mathcal{Y}\}_N$ , the dynamic  
 332 ANTK, which is derived from performing gradient descent on the parameters of an ANN, converges  
 333 pointwise to the importance-adaptive canonical kernel in the dual functional gradient with respect to  
 334 the input sequences. Specifically, it holds that*

$$336 \quad \lim_{t \rightarrow \infty} K_{\theta^t}(\mathbf{S}_i, \cdot) = K(\mathbf{S}_i, \cdot), \quad \forall i \in \mathbb{N}_N. \quad (18)$$

338 This suggests that ANTK, which includes adaptive importance information, serves as a dynamic  
 339 substitute for the importance-adaptive canonical kernel in functional gradient descent with sequence  
 340 inputs, aligning the ANN evolution through parameter gradient descent with that in functional gradient  
 341 descent (Kuk, 1995; Hron et al., 2020; Geifman et al., 2020). This functional insight bridges the  
 342 teaching of attention learners (*i.e.*, ANNs) with that of importance-adaptive nonparametric learners,  
 343 while also facilitating further analysis (*e.g.*, a convex functional  $\mathcal{L}$  retains its convexity with respect  
 344 to  $f_\theta$  from a functional perspective, but is typically nonconvex when considering  $\theta$ ). By utilizing the  
 345 functional insight and applying the canonical kernel (Dou & Liang, 2021) instead of ANTK (which  
 346 should be considered *alongside the remainder*), it facilitates deriving sufficient reduction concerning  
 347  $\mathcal{L}$  in Proposition 4, with the proof deferred to Appendix B.2.

348 **Proposition 4.** *(Sufficient Loss Reduction) Let the convex loss  $\mathcal{L}$  be Lipschitz smooth with a constant  
 349  $\tau > 0$ , and suppose the importance-adaptive canonical kernel is bounded above by a constant  
 350  $\gamma > 0$ . If the learning rate  $\eta$  satisfies  $\eta \leq 1/(2\tau\gamma)$ , then a sufficient reduction in  $\mathcal{L}$  is guaranteed, as  
 351 demonstrated by*

$$352 \quad \frac{\partial \mathcal{L}}{\partial t} \leq -\frac{\eta\gamma}{2} \left( \frac{1}{NS} \sum_{i=1}^N \sum_{j=1}^S \frac{\partial \mathcal{L}(f_{\theta^t}(\mathbf{S}_i)_{(j,:)}, \mathbf{y}_i)_{(j,:)}}{\partial f_{\theta^t}(\mathbf{S}_i)_{(j,:)}} \right)^2. \quad (19)$$

356 This indicates that the variation of  $\mathcal{L}$  over time is capped by a negative value, meaning it decreases by  
 357 at least the magnitude of this upper bound as time progresses, ensuring convergence.

### 359 4.3 THE ATTENT ALGORITHM

361 Building on the understanding of how attention adaptively assigns varying importance in parameter-  
 362 based gradient descent, as well as the consistency between teaching an ANN and a nonparametric  
 363 learner, we introduce the AtteNT algorithm. This algorithm is designed to amplify the steepness of  
 364 the gradients, thereby improving the learning efficiency of the ANN. By considering the gradient as  
 365 the sum of projections of  $\frac{\partial \mathcal{L}(f_\theta, f^*)}{\partial f_\theta}$  onto the basis  $\{K(\mathbf{S}_i, \cdot)\}_N$ , the gradient can be increased simply  
 366 by maximizing the projection  $\frac{\partial \mathcal{L}(f_\theta(\mathbf{S}_i), \mathbf{y}_i)}{\partial f_\theta(\mathbf{S}_i)}$ , thus eliminating the need to compute the norm of the  
 367 basis  $\|K(\mathbf{S}_i, \cdot)\|_{\mathcal{H}}$  (Wright, 2015; Zhang et al., 2024a). This suggests that selecting sequences that  
 368 either maximize  $\left\| \frac{\partial \mathcal{L}(f_\theta(\mathbf{S}_i), \mathbf{y}_i)}{\partial f_\theta(\mathbf{S}_i)} \right\|_2$  or correspond to the larger components of  $\frac{\partial \mathcal{L}(f_\theta, f^*)}{\partial f_\theta}$  can effectively  
 369 amplify the gradient, indicating that

$$370 \quad \{\mathbf{S}_i\}_m^* = \arg \max_{\{\mathbf{S}_i\}_m \subseteq \{\mathbf{S}_i\}_N} \left\| \left[ \frac{\partial \mathcal{L}(f_\theta(\mathbf{S}_i), \mathbf{y}_i)}{\partial f_\theta(\mathbf{S}_i)} \right]_m \right\|_{\mathcal{F}}, \quad (20)$$

374 with Frobenius norm  $\|\cdot\|_{\mathcal{F}}$ . From a functional viewpoint, for a convex loss functional  $\mathcal{L}$ , the norm of  
 375 its partial derivative w.r.t.  $f_\theta$ , denoted as  $\|\frac{\partial \mathcal{L}(f_\theta)}{\partial f_\theta}\|_{\mathcal{H}}$ , is positively correlated with  $\|f_\theta - f^*\|_{\mathcal{H}}$ . As  $f_\theta$   
 376 gets closer to  $f^*$ , the value of  $\|\frac{\partial \mathcal{L}(f_\theta)}{\partial f_\theta}\|_{\mathcal{H}}$  decreases (Boyd & Vandenberghe, 2004; Coleman, 2012).  
 377 This relationship becomes especially prominent when  $\mathcal{L}$  is strongly convex with a larger convexity

constant (Kakade & Tewari, 2008; Arjevani et al., 2016). Building on these insights, the AtteNT algorithm selects sequences by

$$\{\mathcal{S}_i\}_m^* = \arg \max_{\{\mathcal{S}_i\}_m \subseteq \{\mathcal{S}_i\}_N} \|[f_\theta(\mathcal{S}_i) - f^*(\mathcal{S}_i)]_m\|_{\mathcal{F}}. \quad (21)$$

The pseudocode is provided in Algorithm 1.

## 5 EXPERIMENTS AND RESULTS

To demonstrate the broad effectiveness of the AtteNT Algorithm, we conducted extensive experiments across diverse domains. Our evaluation covered large language models and computer vision models. In addition, we validated performance under multiple training paradigms, including training from scratch, and fine-tuning, consistently achieving strong results.

**LLM Scenario.** We evaluate AtteNT algorithms across a diverse set of natural language generation (NLG) tasks. Specifically, we fine-tune LLaMA 2-7B (Touvron et al., 2023), Mistral-7B (Jiang et al., 2023), and Gemma-7B (Team et al., 2024) on the MetaMathQA dataset (Yu et al., 2023a) to benchmark their mathematical reasoning capabilities on GSM8K (Cobbe et al., 2021) and MATH (Hendrycks et al., 2021). To assess coding proficiency, we further fine-tune these models on CodeFeedback (Zheng et al., 2024b) and evaluate on HumanEval (Chen et al., 2021a) and MBPP (Austin et al., 2021). For conversational ability, we train on WizardLM-Evol-Instruct (Xu et al., 2023) and evaluate on MT-Bench (Zheng et al., 2024a). All experiments are conducted on standardized subsets to ensure comparable training efficiency and are trained for five epochs.

As shown in Table 1, AtteNT consistently outperforms standard fine-tuning across all evaluated models and tasks while reducing computational overhead. Specifically, fine-tuning LLaMA, Mistral, and Gemma with AtteNT yields accuracy gains of 1.39, 2.14, and 2.42 on GSM8K, and 1.59, 2.89, and 0.76 on MATH. On coding benchmarks, AtteNT improves performance by 3.66%, 3.25%, and 0.29% on HumanEval, and by 2.08%, 3.25%, and 3.31% on MBPP. We further report average fine-tuning time per model under identical data volumes and epoch settings. Since runtime variation arises primarily from AtteNT’s adaptive data selection, the observed results highlight its efficiency: on average, AtteNT reduces training time by 12.78%, underscoring its advantage in both performance and resource savings.

**CV Scenario.** The Multi-Modal MAE (Bachmann et al., 2022) is designed to address a diverse range of downstream tasks by employing three specialized encoders, each dedicated to processing a distinct image modality. During pre-training, we explore various selection strategies, including different ratios and intervals, to optimize model configuration. The pretraining process is conducted over 800 epochs.

For unsupervised pre-training, we utilize ImageNetS50 (Gao et al., 2021) to evaluate the effectiveness of the AtteNT method in enhancing the performance of downstream tasks under suboptimal conditions. Classification performance is assessed using the validation subset of the original dataset, while semantic segmentation and depth estimation tasks are fine-tuned and evaluated on the NYUv2 dataset (Silberman et al., 2012). Given the absence of a large multi-task dataset with aligned task-specific images (Doersch & Zisserman, 2017; Bachmann et al., 2022; Wang et al., 2023), we generate pseudo-labels for ImageNetS50 using Mask2Former (Cheng et al., 2022).

Table 1: AtteNT on NLG tasks. The results are averaged over three runs, with standard deviations included. The GSM8K and MATH datasets share a math fine-tuned model, while HumanEval and MBPP use a code fine-tuned model. MT-Bench utilizes a conversation fine-tuned model. The "Avg. time" represents the average fine-tuning time for the three models.

Model	AtteNT	Avg. Time( $\downarrow$ )	GSM8K( $\uparrow$ )	MATH( $\uparrow$ )	HumanEval( $\uparrow$ )	MBPP( $\uparrow$ )	MT-Bench( $\uparrow$ )
LLaMA 2-7B	w/o	246 $\pm$ 1m	42.96 $\pm$ 0.12	5.06 $\pm$ 0.16	18.35 $\pm$ 0.31	35.65 $\pm$ 0.25	<b>4.58<math>\pm</math>0.01</b>
	w	<b>213<math>\pm</math>2m</b>	<b>43.45<math>\pm</math>0.55</b>	<b>6.48<math>\pm</math>0.24</b>	<b>21.80<math>\pm</math>0.38</b>	<b>37.61<math>\pm</math>0.42</b>	4.49 $\pm$ 0.02
Mistral-7B	w/o	204 $\pm$ 2m	69.13 $\pm$ 0.22	20.06 $\pm$ 0.20	43.42 $\pm$ 0.14	58.52 $\pm$ 0.13	5.03 $\pm$ 0.05
	w	<b>180<math>\pm</math>2m</b>	<b>71.26<math>\pm</math>0.23</b>	<b>23.12<math>\pm</math>0.44</b>	<b>46.55<math>\pm</math>0.25</b>	<b>61.74<math>\pm</math>0.54</b>	<b>5.32<math>\pm</math>0.04</b>
Gemma-7B	w/o	228 $\pm$ 2m	75.23 $\pm$ 0.45	30.52 $\pm$ 0.48	53.83 $\pm$ 0.27	65.69 $\pm$ 0.29	5.42 $\pm$ 0.04
	w	<b>201<math>\pm</math>2m</b>	<b>77.74<math>\pm</math>0.32</b>	<b>31.40<math>\pm</math>0.36</b>	<b>54.26<math>\pm</math>0.28</b>	<b>66.28<math>\pm</math>0.46</b>	<b>5.44<math>\pm</math>0.08</b>

432  
 433 Table 2: AtteNT across various CV downstream tasks. ImageNetS50 uses 50 categories from ImageNet  
 434 for classification, evaluated by accuracy. NYUv2(S) is a semantic segmentation task with mIoU as  
 435 the metric. NYUv2(D) involves depth estimation, evaluated using the  $\delta_1$  metric, which measures the  
 436 percentage of pixels with an error ratio below 1.25 (Doersch & Zisserman, 2017).

437 Model	438 AtteNT	439 Pretraining Time( $\downarrow$ )	440 ImageNetS50( $\uparrow$ )	441 NYUv2(S)( $\uparrow$ )	442 NYUv2(D)( $\uparrow$ )
438 Multi-Modal MAE	439 w/o	440 1234m	441 92.2	442 51.9	443 52.1
	w	<b>980m</b> (-20.58%)	<b>92.3</b>	<b>52.6</b>	<b>57.2</b>

443 Table 3: Ablation study of AtteNT pre-training configurations. Ratio controls how the fraction of  
 444 selected samples increases over epochs. Interval denotes how often the subset is re-sampled. Selection  
 445 specifies the sampling strategy: Random (no difficulty prior), Hard (selects only difficult samples),  
 446 and Soft (Gumbel-Top-k difficulty-aware sampling). The configuration (Incremental, Incremental,  
 447 Soft) in the red color row is adopted as our final AtteNT setting, as it simultaneously reduces  
 448 pre-training time and improves performance on all downstream tasks.

448 Ratio	449 Interval	450 Selection	451 Pre-training		452 Downstream		
			453 Training time( $\downarrow$ )	454 ImageNetS50( $\uparrow$ )	455 NYUv2(S)( $\uparrow$ )	456 NYUv2(D)( $\uparrow$ )	
-	-	-	1234m	92.2	51.9	52.1	
Cosine	Incremental	Random	966m	88.6	45.3	49.6	
Cosine	Incremental	Soft	995m	92.1	52.2	58.8	
Cosine	Fixed	Soft	1301m	<b>93.2</b>	53.6	61.4	
Incremental	Incremental	Soft	<b>980m</b>	92.3	52.6	<b>57.2</b>	
Incremental	Fixed	Soft	1319m	92.4	<b>53.7</b>	<b>62.1</b>	
Cosine	Incremental	Hard	972m	91.8	49.5	57.3	
Cosine	Fixed	Hard	1285m	92.1	53.0	60.8	
Incremental	Incremental	Hard	<b>963m</b>	91.4	48.4	57.2	
Incremental	Fixed	Hard	1302m	92.5	52.7	59.5	

457  
 458 As shown in Table 2, the AtteNT strategy results in a significant reduction in training time, saving  
 459 20.58% during long-duration training from scratch. Additionally, it consistently improves per-  
 460 formance across a wide range of downstream tasks. Notably, the depth estimation task exhibits the  
 461 largest gain, achieving a 5.1% improvement. We attribute this improvement to the nature of the  
 462 depth estimation task, which is independent of image type, thus preventing any disruption in data  
 463 distribution during the selection process. Our experiments demonstrate the efficacy of AtteNT within  
 464 the ViT architecture.

465  
 466 The practical performance gains stem directly from the curriculum effect induced by nonparametric  
 467 teaching (Bengio et al., 2009; Wang et al., 2021b; Zhang et al., 2023b; 2025), which greedily selects  
 468 the examples that most advance the learner. This naturally creates a curriculum that focuses training  
 469 on informative, high-gradient examples and avoids gradient dilution from already-mastered ones.

470  
 471 We further present the ablation study results for AtteNT, focusing on the effects of varying data  
 472 selection strategies and their impact on downstream tasks. Specifically, we investigate the influence  
 473 of dynamic changes in data selection ratios and step sizes, following the strategy proposed in (Zhang  
 474 et al., 2023b). Additionally, we examine how different selection strategies affect the performance  
 475 of downstream tasks. The Random strategy involves selecting data without any predefined criteria,  
 476 while the Hard strategy entails deterministic data selection. The Soft strategy, on the other hand,  
 477 uses probability-based data selection, derived from loss scores. To implement this, we apply the  
 478 Gumbel-Top-k selection algorithm (Kool et al., 2019) for sampling without replacement. Our results  
 479 show that the Soft selection strategy achieves the best performance in downstream tasks, significantly  
 480 improving the model’s robustness during training. A more detailed study of the sample ratio can be  
 481 found in Appendix D.1, and additional comparison results are provided in Appendix D.2.

## 482 6 CONCLUDING REMARKS AND FUTURE WORK

483  
 484 This paper introduces AtteNT, a novel paradigm that enhances the learning efficiency of attention  
 485 learners (*i.e.*, ANNs) through nonparametric teaching theory. Specifically, AtteNT reduces the  
 486 wallclock time required to learn the implicit mapping from sequences to relevant properties by

486 13.01% to 20.58% while consistently preserving and often enhancing the performance across a  
 487 diverse set of downstream tasks. Moreover, AtteNT establishes a theoretical connection between the  
 488 evolution of an ANN via parameter-based gradient descent and that of a function using functional  
 489 gradient descent in nonparametric teaching. This connection between nonparametric teaching theory  
 490 and ANN training expands the potential applications of nonparametric teaching in contexts that  
 491 involve attention mechanisms.

492 In future work, it would be interesting to explore other variations of AtteNT for different attention  
 493 learners, such as graph attention networks (Veličković et al., 2018). Additionally, investigating its  
 494 robustness under real-world label noise, building upon recent noise-robust advancements (Wei et al.,  
 495 2024; Hu et al., 2024), could yield crucial improvements. Another promising direction is to examine  
 496 the practical applications of AtteNT in improving the efficiency of data-driven methods (Henaff,  
 497 2020; Touvron et al., 2021; Müller et al., 2022) for attention-related tasks, especially in areas like  
 498 world models.

499

500 

## REPRODUCIBILITY STATEMENT

501

502 We have taken substantial steps to promote the reproducibility of our research. Appendix A offers  
 503 a comprehensive overview of the notation, theoretical background, and key algorithm. All proofs  
 504 for theorems and propositions can be found in Appendix B. Meanwhile, Appendix C provides a  
 505 comprehensive description of the experimental setup, including training configurations, hyperparam-  
 506 eter choices, algorithmic details, and dataset preprocessing procedures. Codes are available at the  
 507 following anonymous link: [LINK](#).

508

509

510 

## REFERENCES

511

511 Subutai Ahmad. VISIT: a neural model of covert visual attention. In *NeurIPS*, 1991. 1

512 Scott Alfeld, Xiaojin Zhu, and Paul Barford. Explicit defense actions against test-set attacks. In  
 513 *AAAI*, 2017. 3

514 Yossi Arjevani, Shai Shalev-Shwartz, and Ohad Shamir. On lower and upper bounds in smooth and  
 515 strongly convex optimization. *The Journal of Machine Learning Research*, 17(1):4303–4353, 2016.  
 516 8

517 Anurag Arnab, Mostafa Dehghani, Georg Heigold, Chen Sun, Mario Lučić, and Cordelia Schmid.  
 518 ViViT: A video vision transformer. In *Proceedings of the IEEE/CVF international conference on  
 519 computer vision*, pp. 6836–6846, 2021. 2

520 Jacob Austin, Augustus Odena, Maxwell Nye, Maarten Bosma, Henryk Michalewski, David Dohan,  
 521 Ellen Jiang, Carrie Cai, Michael Terry, Quoc Le, and Charles Sutton. Program synthesis with large  
 522 language models. *arXiv preprint arXiv:2108.07732*, 2021. 8

523 Reza Azad, Leon Niggemeier, Michael Hüttemann, Amirhossein Kazerouni, Ehsan Khodapanah  
 524 Aghdam, Yury Velichko, Ulas Bagci, and Dorit Merhof. Beyond self-attention: Deformable large  
 525 kernel attention for medical image segmentation. In *WACV*, 2024. 1

526 Roman Bachmann, David Mizrahi, Andrei Atanov, and Amir Zamir. Multimae: Multi-modal multi-  
 527 task masked autoencoders. In *European Conference on Computer Vision (ECCV)*, pp. 348–367.  
 528 Springer, 2022. 8

529 Dzmitry Bahdanau, Kyung Hyun Cho, and Yoshua Bengio. Neural machine translation by jointly  
 530 learning to align and translate. In *ICLR*, 2015. 1, 2, 3

531 Max Bain, Arsha Nagrani, Gü̈l Varol, and Andrew Zisserman. Frozen in time: A joint video and  
 532 image encoder for end-to-end retrieval. In *Proceedings of the IEEE/CVF international conference  
 533 on computer vision*, pp. 1728–1738, 2021. 1

534 Iz Beltagy, Kyle Lo, and Arman Cohan. SciBERT: A pretrained language model for scientific text.  
 535 In *EMNLP-IJCNLP*, 2019. 1

540    Yoshua Bengio, Jérôme Louradour, Ronan Collobert, and Jason Weston. Curriculum learning. In  
 541    *ICML*, 2009. 9

542

543    Stephen Boyd and Lieven Vandenberghe. *Convex optimization*. Cambridge university press, 2004. 7

544

545    Nicola Cancedda, Eric Gaussier, Cyril Goutte, and Jean-Michel Renders. Word-sequence kernels.  
 546    *Journal of machine learning research*, 3(Feb):1059–1082, 2003. 3, 7

547

548    Mark Chen, Jerry Tworek, Heewoo Jun, Qiming Yuan, Henrique Ponde de Oliveira Pinto, Jared  
 549    Kaplan, Harri Edwards, Yuri Burda, Nicholas Joseph, Greg Brockman, Alex Ray, Raul Puri,  
 550    Gretchen Krueger, Michael Petrov, Heidy Khlaaf, Girish Sastry, Pamela Mishkin, Brooke Chan,  
 551    Scott Gray, Nick Ryder, Mikhail Pavlov, Alethea Power, Lukasz Kaiser, Mohammad Bavarian,  
 552    Clemens Winter, Philippe Tillet, Felipe Petroski Such, Dave Cummings, Matthias Plappert, Fotios  
 553    Chantzis, Elizabeth Barnes, Ariel Herbert-Voss, William Hebbgen Guss, Alex Nichol, Alex Paino,  
 554    Nikolas Tezak, Jie Tang, Igor Babuschkin, Suchir Balaji, Shantanu Jain, William Saunders,  
 555    Christopher Hesse, Andrew N. Carr, Jan Leike, Josh Achiam, Vedant Misra, Evan Morikawa,  
 556    Alec Radford, Matthew Knight, Miles Brundage, Mira Murati, Katie Mayer, Peter Welinder, Bob  
 557    McGrew, Dario Amodei, Sam McCandlish, Ilya Sutskever, and Wojciech Zaremba. Evaluating  
 558    large language models trained on code. *arXiv preprint arXiv:2107.03374*, 2021a. 8

559

560    Tianlong Chen, Yu Cheng, Zhe Gan, Lu Yuan, Lei Zhang, and Zhangyang Wang. Chasing sparsity  
 561    in vision transformers: An end-to-end exploration. *Advances in Neural Information Processing  
 562    Systems*, 34:19974–19988, 2021b. 2

563

564    Xiaohan Chen, Yu Cheng, Shuohang Wang, Zhe Gan, Zhangyang Wang, and Jingjing Liu. EarlyBERT:  
 565    Efficient BERT training via early-bird lottery tickets. In *Proceedings of the 59th Annual Meeting  
 566    of the Association for Computational Linguistics and the 11th International Joint Conference on  
 567    Natural Language Processing (Volume 1: Long Papers)*, pp. 2195–2207, 2021c. 2

568

569    Yuantao Chen, Runlong Xia, Kai Yang, and Ke Zou. Dnnam: Image inpainting algorithm via deep  
 570    neural networks and attention mechanism. *Applied Soft Computing*, 154:111392, 2024. 1

571

572    Zhao Chen, Vijay Badrinarayanan, Chen-Yu Lee, and Andrew Rabinovich. Gradnorm: Gradient  
 573    normalization for adaptive loss balancing in deep multitask networks. In *International Conference  
 574    on Machine Learning (ICML)*, 2018. 33, 34

575

576    Bowen Cheng, Ishan Misra, Alexander G. Schwing, Alexander Kirillov, and Rohit Girdhar. Masked-  
 577    attention mask transformer for universal image segmentation. In *CVPR*, 2022. 8, 31

578

579    Karl Cobbe, Vineet Kosaraju, Mohammad Bavarian, Mark Chen, Heewoo Jun, Lukasz Kaiser,  
 580    Matthias Plappert, Jerry Tworek, Jacob Hilton, Reiichiro Nakano, Christopher Hesse, and John  
 581    Schulman. Training verifiers to solve math word problems. *arXiv preprint arXiv:2110.14168*,  
 582    2021. 8

583

584    Rodney Coleman. *Calculus on normed vector spaces*. Springer Science & Business Media, 2012. 4,  
 585    7, 19

586

587    Micaela E Consens, Cameron Dufault, Michael Wainberg, Duncan Forster, Mehran Karimzadeh,  
 588    Hani Goodarzi, Fabian J Theis, Alan Moses, and Bo Wang. Transformers and genome language  
 589    models. *Nature Machine Intelligence*, pp. 1–17, 2025. 1

590

591    Dorottya Demszky, Diyi Yang, David S Yeager, Christopher J Bryan, Margaret Clapper, Susannah  
 592    Chandhok, Johannes C Eichstaedt, Cameron Hecht, Jeremy Jamieson, Meghann Johnson, Michaela  
 593    Jones, Danielle Krettek-Cobb, Leslie Lai, Nirel Jones Mitchell, Desmond C. Ong, Carol S. Dweck,  
 594    James J. Gross, and James W. Pennebaker. Using large language models in psychology. *Nature  
 595    Reviews Psychology*, 2(11):688–701, 2023. 2

596

597    Jacob Devlin, Ming-Wei Chang, Kenton Lee, and Kristina Toutanova. Bert: Pre-training of deep  
 598    bidirectional transformers for language understanding. In *NAACL*, 2019. 1

594 Hantian Ding, Zijian Wang, Giovanni Paolini, Varun Kumar, Anoop Deoras, Dan Roth, and Stefano  
 595 Soatto. Fewer truncations improve language modeling. In *International Conference on Machine*  
 596 *Learning*, pp. 11030–11048. PMLR, 2024. 5

597

598 Carl Doersch and Andrew Zisserman. Multi-task self-supervised visual learning. In *International*  
 599 *Conference on Computer Vision (ICCV)*, 2017. 8, 9

600 Yihe Dong, Jean-Baptiste Cordonnier, and Andreas Loukas. Attention is not all you need: Pure  
 601 attention losses rank doubly exponentially with depth. In *International conference on machine*  
 602 *learning*, pp. 2793–2803. PMLR, 2021. 4

603

604 Alexey Dosovitskiy, Lucas Beyer, Alexander Kolesnikov, Dirk Weissenborn, Xiaohua Zhai, Thomas  
 605 Unterthiner, Mostafa Dehghani, Matthias Minderer, Georg Heigold, Sylvain Gelly, Jakob Uszkoreit,  
 606 and Neil Houlsby. An image is worth 16x16 words: Transformers for image recognition at scale.  
 607 In *International Conference on Learning Representations*, 2020. 1, 2, 31

608

609 Xialiang Dou and Tengyuan Liang. Training neural networks as learning data-adaptive kernels: Prov-  
 610 able representation and approximation benefits. *Journal of the American Statistical Association*,  
 611 116(535):1507–1520, 2021. 7

612

613 Stéphane d’Ascoli, Hugo Touvron, Matthew L Leavitt, Ari S Morcos, Giulio Biroli, and Levent Sagun.  
 614 ConViT: Improving vision transformers with soft convolutional inductive biases. In *International*  
 615 *conference on machine learning*, pp. 2286–2296. PMLR, 2021. 2

616

617 Jeffrey L Elman. Finding structure in time. *Cognitive science*, 14(2):179–211, 1990. 6

618

619 Jonathan Frankle and Michael Carbin. The lottery ticket hypothesis: Finding sparse, trainable neural  
 620 networks. In *International Conference on Learning Representations*, 2018. 2

621

622 Andrea Galassi, Marco Lippi, and Paolo Torroni. Attention in natural language processing. *IEEE*  
 623 *transactions on neural networks and learning systems*, 32(10):4291–4308, 2020. 2

624

625 Shang-Hua Gao, Zhong-Yu Li, Ming-Hsuan Yang, Ming-Ming Cheng, Junwei Han, and Philip Torr.  
 626 Large-scale unsupervised semantic segmentation. *arXiv preprint arXiv:2106.03149*, 2021. 8, 31

627

628 Amnon Geifman, Abhay Yadav, Yoni Kasten, Meirav Galun, David Jacobs, and Basri Ronen. On the  
 629 similarity between the laplace and neural tangent kernels. In *NeurIPS*, 2020. 7

630

631 Izrail Moiseevitch Gelfand and Richard A Silverman. *Calculus of variations*. Courier Corporation,  
 632 2000. 19

633

634 Golnaz Ghiasi, Yin Cui, Aravind Srinivas, Rui Qian, Tsung-Yi Lin, Ekin D Cubuk, Quoc V Le, and  
 635 Barret Zoph. Simple copy-paste is a strong data augmentation method for instance segmentation.  
 636 In *Conference on Computer Vision and Pattern Recognition (CVPR)*, pp. 2918–2928, 2021. 32

637

638 Yu Gu, Robert Tinn, Hao Cheng, Michael Lucas, Naoto Usuyama, Xiaodong Liu, Tristan Naumann,  
 639 Jianfeng Gao, and Hoifung Poon. Domain-specific language model pretraining for biomedical  
 640 natural language processing. *ACM Transactions on Computing for Healthcare (HEALTH)*, 3(1):  
 641 1–23, 2021. 1

642

643 Mohammed Hassanin, Saeed Anwar, Ibrahim Radwan, Fahad Shahbaz Khan, and Ajmal Mian. Visual  
 644 attention methods in deep learning: An in-depth survey. *Information Fusion*, 108:102417, 2024. 2

645

646 Olivier Henaff. Data-efficient image recognition with contrastive predictive coding. In *ICML*, 2020.  
 647 10

648

649 Dan Hendrycks, Collin Burns, Saurav Kadavath, Akul Arora, Steven Basart, Eric Tang, Dawn Song,  
 650 and Jacob Steinhardt. Measuring mathematical problem solving with the math dataset. *arXiv*  
 651 *preprint arXiv:2103.03874*, 2021. 8

652

653 Jiri Hron, Yasaman Bahri, Jascha Sohl-Dickstein, and Roman Novak. Infinite attention: NNGP  
 654 and NTK for deep attention networks. In *International Conference on Machine Learning*, pp.  
 655 4376–4386. PMLR, 2020. 2, 5, 6, 7, 25

648 Yuchen Hu, CHEN CHEN, Chao-Han Huck Yang, Ruizhe Li, Chao Zhang, Pin-Yu Chen, and  
 649 EngSiong Chng. Large language models are efficient learners of noise-robust speech recognition.  
 650 In *ICLR*, 2024. 10

651 Gao Huang, Yu Sun, Zhuang Liu, Daniel Sedra, and Kilian Q Weinberger. Deep networks with  
 652 stochastic depth. In *European Conference on Computer Vision (ECCV)*, pp. 646–661. Springer,  
 653 2016. 32

654 Xiao Shi Huang, Felipe Perez, Jimmy Ba, and Maksims Volkovs. Improving transformer optimization  
 655 through better initialization. In *International Conference on Machine Learning*, pp. 4475–4483.  
 656 PMLR, 2020. 2

657 Arthur Jacot, Franck Gabriel, and Clément Hongler. Neural tangent kernel: Convergence and  
 658 generalization in neural networks. *Advances in Neural Information Processing Systems (NeurIPS)*,  
 659 2018. 5, 6, 25

660 Albert Q. Jiang, Alexandre Sablayrolles, Arthur Mensch, Chris Bamford, Devendra Singh Chaplot,  
 661 Diego de Las Casas, Florian Bressand, Gianna Lengyel, Guillaume Lample, Lucile Saulnier,  
 662 Lélio Renard Lavaud, Marie-Anne Lachaux, Pierre Stock, Teven Le Scao, Thibaut Lavril, Thomas  
 663 Wang, Timothée Lacroix, and William El Sayed. Mistral 7b. *arXiv preprint arXiv:2310.06825*,  
 664 2023. 8

665 Mingyu Jin, Qinkai Yu, Dong Shu, Haiyan Zhao, Wenyue Hua, Yanda Meng, Yongfeng Zhang, and  
 666 Mengnan Du. The impact of reasoning step length on large language models. In *ACL (Findings)*,  
 667 2024. 2

668 Michael I Jordan. Serial order: A parallel distributed processing approach. In *Advances in psychology*,  
 669 volume 121, pp. 471–495. Elsevier, 1997. 6

670 Tokio Kajitsuka and Issei Sato. Are transformers with one layer self-attention using low-rank  
 671 weight matrices universal approximators? In *The Twelfth International Conference on Learning  
 672 Representations*, 2024. 4

673 Sham M Kakade and Ambuj Tewari. On the generalization ability of online strongly convex  
 674 programming algorithms. In *NeurIPS*, 2008. 8

675 Angelos Katharopoulos and François Fleuret. Not all samples are created equal: Deep learning with  
 676 importance sampling. In *International conference on machine learning*, pp. 2525–2534. PMLR,  
 677 2018. 33

678 Angelos Katharopoulos, Apoorv Vyas, Nikolaos Pappas, and François Fleuret. Transformers are  
 679 RNNs: Fast autoregressive transformers with linear attention. In *International conference on  
 680 machine learning*, pp. 5156–5165. PMLR, 2020. 2

681 Franz J Király and Harald Oberhauser. Kernels for sequentially ordered data. *Journal of Machine  
 682 Learning Research*, 20(31):1–45, 2019. 3, 7

683 Nikita Kitaev, Lukasz Kaiser, and Anselm Levskaya. Reformer: The efficient transformer. In  
 684 *International Conference on Learning Representations*, 2020. 2

685 Qiuqiang Kong, Changsong Yu, Yong Xu, Turab Iqbal, Wenwu Wang, and Mark D Plumley. Weakly  
 686 labelled audioset tagging with attention neural networks. *IEEE/ACM Transactions on Audio,  
 687 Speech, and Language Processing*, 27(11):1791–1802, 2019. 1, 2

688 Wouter Kool, Herke Van Hoof, and Max Welling. Stochastic beams and where to find them: The  
 689 Gumbel-top- $k$  trick for sampling sequences without replacement. In *International conference on  
 690 machine learning*, pp. 3499–3508. PMLR, 2019. 9

691 Anthony YC Kuk. Asymptotically unbiased estimation in generalized linear models with random  
 692 effects. *Journal of the Royal Statistical Society Series B: Statistical Methodology*, 57(2):395–407,  
 693 1995. 7

694 Peter D Lax. *Functional analysis*. John Wiley & Sons, 2014. 3

702 Juho Lee, Yoonho Lee, Jungtaek Kim, Adam Kosiorek, Seungjin Choi, and Yee Whye Teh. Set trans-  
 703 former: A framework for attention-based permutation-invariant neural networks. In *International*  
 704 *conference on machine learning*, pp. 3744–3753. PMLR, 2019. 6

705 Jeffrey Li, Alex Fang, Georgios Smyrnis, Maor Ivgi, Matt Jordan, Samir Yitzhak Gadre, Hritik Bansal,  
 706 Etash Kumar Guha, Sedrick Keh, Kushal Arora, Saurabh Garg, Rui Xin, Niklas Muennighoff,  
 707 Reinhard Heckel, Jean Mercat, Mayee F. Chen, Suchin Gururangan, Mitchell Wortsman, Alon  
 708 Albalak, Yonatan Bitton, Marianna Nezhurina, Amro Abbas, Cheng-Yu Hsieh, Dhruba Ghosh,  
 709 Josh Gardner, Maciej Kilian, Hanlin Zhang, Rulin Shao, Sarah M. Pratt, Sunny Sanyal, Gabriel  
 710 Ilharco, Giannis Daras, Kalyani Marathe, Aaron Gokaslan, Jieyu Zhang, Khyathi Raghavi Chandu,  
 711 Thao Nguyen, Igor Vasiljevic, Sham M. Kakade, Shuran Song, Sujay Sanghavi, Fartash Faghri,  
 712 Sewoong Oh, Luke Zettlemoyer, Kyle Lo, Alaaeldin El-Nouby, Hadi Pouransari, Alexander  
 713 Toshev, Stephanie Wang, Dirk Groeneveld, Luca Soldaini, Pang Wei Koh, Jenia Jitsev, Thomas  
 714 Kollar, Alexandros G. Dimakis, Yair Carmon, Achal Dave, Ludwig Schmidt, and Vaishaal Shankar.  
 715 DataComp-LM: In search of the next generation of training sets for language models. In *NeurIPS*,  
 716 volume 37, pp. 14200–14282, 2024. Datasets and Benchmarks Track. 1, 2

717 Zonglin Li, Chong You, Srinadh Bhojanapalli, Daliang Li, Ankit Singh Rawat, Sashank J. Reddi,  
 718 Ke Ye, Felix Chern, Felix X. Yu, Ruiqi Guo, and Sanjiv Kumar. The lazy neuron phenomenon: On  
 719 emergence of activation sparsity in transformers. In *The Eleventh International Conference on*  
 720 *Learning Representations*, 2023. 2

721 Tianyang Lin, Yuxin Wang, Xiangyang Liu, and Xipeng Qiu. A survey of transformers. *AI open*, 3:  
 722 111–132, 2022. 2

723 Zhenghao Lin, Zhibin Gou, Yeyun Gong, Xiao Liu, yelong shen, Ruochen Xu, Chen Lin, Yujiu Yang,  
 724 Jian Jiao, Nan Duan, and Weizhu Chen. Not all tokens are what you need for pretraining. *Advances*  
 725 *in Neural Information Processing Systems*, 37:29029–29063, 2024. 2, 31, 33

726 Qiang Liu. Stein variational gradient descent as gradient flow. In *NeurIPS*, 2017. 4

727 Qiang Liu and Dilin Wang. Stein variational gradient descent: A general purpose bayesian inference  
 728 algorithm. In *NeurIPS*, 2016. 3

729 Weiyang Liu, Bo Dai, Ahmad Humayun, Charlene Tay, Chen Yu, Linda B Smith, James M Rehg,  
 730 and Le Song. Iterative machine teaching. In *ICML*, 2017. 1, 3

731 Weiyang Liu, Bo Dai, Xingguo Li, Zhen Liu, James Rehg, and Le Song. Towards black-box iterative  
 732 machine teaching. In *ICML*, 2018a. 1, 3

733 Xin Liu, Qingcai Chen, Chong Deng, Huajun Zeng, Jing Chen, Dongfang Li, and Buzhou Tang.  
 734 Lcqmc: A large-scale chinese question matching corpus. In *Proceedings of the 27th international*  
 735 *conference on computational linguistics*, pp. 1952–1962, 2018b. 1

736 Ilya Loshchilov and Frank Hutter. SGDR: Stochastic gradient descent with warm restarts. In  
 737 *International Conference on Learning Representations (ICLR)*, 2017. 31

738 Jiachen Lu, Jinghan Yao, Junge Zhang, Xiatian Zhu, Hang Xu, Weiguo Gao, Chunjing Xu, Tao  
 739 Xiang, and Li Zhang. SOFT: Softmax-free transformer with linear complexity. *Advances in Neural*  
 740 *Information Processing Systems*, 34:21297–21309, 2021. 2

741 Ziyuan Luo, Boxin Shi, Haoliang Li, and Renjie Wan. Imaging interiors: An implicit solution to  
 742 electromagnetic inverse scattering problems. In *ECCV*, 2024. 3

743 Yuzhe Ma, Xuezhou Zhang, Wen Sun, and Jerry Zhu. Policy poisoning in batch reinforcement  
 744 learning and control. In *NeurIPS*, 2019. 3

745 Arvind V Mahankali, Tatsunori Hashimoto, and Tengyu Ma. One step of gradient descent is provably  
 746 the optimal in-context learner with one layer of linear self-attention. In *The Twelfth International*  
 747 *Conference on Learning Representations*, 2024. 4

748 Ashok Vardhan Makkula, Marco Bondaschi, Adway Girish, Alliot Nagle, Martin Jaggi, Hyeji Kim,  
 749 and Michael Gastpar. Attention with Markov: A curious case of single-layer transformers. In *The*  
 750 *Thirteenth International Conference on Learning Representations*, 2025. 4

756 Fanxu Meng, Zhaohui Wang, and Muhan Zhang. PiSSA: Principal singular values and singular  
 757 vectors adaptation of large language models. *arXiv preprint arXiv:2404.02948*, 2024. 31  
 758

759 Thomas Müller, Alex Evans, Christoph Schied, and Alexander Keller. Instant neural graphics  
 760 primitives with a multiresolution hash encoding. *ACM transactions on graphics (TOG)*, 41(4):  
 761 1–15, 2022. 10

762 Arsha Nagrani, Shan Yang, Anurag Arnab, Aren Jansen, Cordelia Schmid, and Chen Sun. Attention  
 763 bottlenecks for multimodal fusion. In *NeurIPS*, volume 34, pp. 14200–14213, 2021. 1

764 Amin Rakhsha, Goran Radanovic, Rati Devidze, Xiaojin Zhu, and Adish Singla. Policy teaching  
 765 via environment poisoning: Training-time adversarial attacks against reinforcement learning. In  
 766 *ICML*, 2020. 3

767 Bernhard Schölkopf and Alexander J Smola. *Learning with kernels: support vector machines,  
 768 regularization, optimization, and beyond*. MIT press, 2002. 3

769 Piyush Sharma, Nan Ding, Sebastian Goodman, and Radu Soricut. Conceptual captions: A cleaned,  
 770 hypernymed, image alt-text dataset for automatic image captioning. In *Proceedings of the 56th  
 771 Annual Meeting of the Association for Computational Linguistics (Volume 1: Long Papers)*, pp.  
 772 2556–2565, 2018. 1

773 Yan Shu, Zheng Liu, Peitian Zhang, Minghao Qin, Junjie Zhou, Zhengyang Liang, Tiejun Huang,  
 774 and Bo Zhao. Video-XL: Extra-long vision language model for hour-scale video understanding. In  
 775 *Proceedings of the Computer Vision and Pattern Recognition Conference*, pp. 26160–26169, 2025.  
 776 1

777 Nathan Silberman, Derek Hoiem, Pushmeet Kohli, and Rob Fergus. Indoor segmentation and support  
 778 inference from RGBD images. In *European Conference on Computer Vision (ECCV)*, 2012. 8

779 Adish Singla, Ilija Bogunovic, Gábor Bartók, Amin Karbasi, and Andreas Krause. Near-optimally  
 780 teaching the crowd to classify. In *ICML*, 2014. 3

781 Derya Soydancer. Attention mechanism in neural networks: where it comes and where it goes. *Neural  
 782 Computing and Applications*, 34(16):13371–13385, 2022. 1

783 Quan Tang, Bowen Zhang, Jiajun Liu, Fagui Liu, and Yifan Liu. Dynamic token pruning in plain  
 784 vision transformers for semantic segmentation. In *Proceedings of the IEEE/CVF International  
 785 Conference on Computer Vision*, pp. 777–786, 2023. 2

786 Rohan Taori, Ishaan Gulrajani, Tianyi Zhang, Yann Dubois, Xuechen Li, Carlos Guestrin, Percy  
 787 Liang, and Tatsunori B. Hashimoto. Stanford alpaca: An instruction-following LLaMA model.  
 788 [https://github.com/tatsu-lab/stanford\\_alpaca](https://github.com/tatsu-lab/stanford_alpaca), 2023. 31

789 Gemma Team, Thomas Mesnard, Cassidy Hardin, Robert Dadashi, Surya Bhupatiraju, Shreya Pathak,  
 790 Laurent Sifre, Morgane Rivière, Mihir Sanjay Kale, Juliette Love, Pouya Tafti, Léonard Hussonot,  
 791 Pier Giuseppe Sessa, Aakanksha Chowdhery, Adam Roberts, Aditya Barua, Alex Botev, Alex  
 792 Castro-Ros, Ambrose Slone, Amélie Héliou, Andrea Tacchetti, Anna Bulanova, Antonia Paterson,  
 793 Beth Tsai, Bobak Shahriari, Charline Le Lan, Christopher A. Choquette-Choo, Clément Crepy,  
 794 Daniel Cer, Daphne Ippolito, David Reid, Elena Buchatskaya, Eric Ni, Eric Noland, Geng Yan,  
 795 George Tucker, George-Christian Muraru, Grigory Rozhdestvenskiy, Henryk Michalewski, Ian  
 796 Tenney, Ivan Grishchenko, Jacob Austin, James Keeling, Jane Labanowski, Jean-Baptiste Lespiau,  
 797 Jeff Stanway, Jenny Brennan, Jeremy Chen, Johan Ferret, Justin Chiu, Justin Mao-Jones, Katherine  
 798 Lee, Kathy Yu, Katie Millican, Lars Lowe Sjoesund, Lisa Lee, Lucas Dixon, Machel Reid, Maciej  
 799 Mikuła, Mateo Wirth, Michael Sharman, Nikolai Chainaev, Nithum Thain, Olivier Bachem, Oscar  
 800 Chang, Oscar Wahlinez, Paige Bailey, Paul Michel, Petko Yotov, Rahma Chaabouni, Ramona  
 801 Comanescu, Reena Jana, Rohan Anil, Ross McIlroy, Ruibo Liu, Ryan Mullins, Samuel L Smith,  
 802 Sebastian Borgeaud, Sertan Girgin, Sholto Douglas, Shree Pandya, Siamak Shakeri, Soham De,  
 803 Ted Klimenko, Tom Hennigan, Vlad Feinberg, Wojciech Stokowiec, Yu hui Chen, Zafarali Ahmed,  
 804 Zhitao Gong, Tris Warkentin, Ludovic Peran, Minh Giang, Clément Farabet, Oriol Vinyals, Jeff  
 805 Dean, Koray Kavukcuoglu, Demis Hassabis, Zoubin Ghahramani, Douglas Eck, Joelle Barral,  
 806 Fernando Pereira, Eli Collins, Armand Joulin, Noah Fiedel, Evan Senter, Alek Andreev, and  
 807 Kathleen Kenealy. Gemma: Open models based on gemini research and technology. *arXiv preprint  
 808 arXiv:2403.08295*, 2024. 8

810 Arun James Thirunavukarasu, Darren Shu Jeng Ting, Kabilan Elangovan, Laura Gutierrez, Ting Fang  
 811 Tan, and Daniel Shu Wei Ting. Large language models in medicine. *Nature medicine*, 29(8):  
 812 1930–1940, 2023. 2

813

814 Hugo Touvron, Matthieu Cord, Matthijs Douze, Francisco Massa, Alexandre Sablayrolles, and Hervé  
 815 Jégou. Training data-efficient image transformers & distillation through attention. In *ICML*, 2021.  
 816 10

817

818 Hugo Touvron, Louis Martin, Kevin Stone, Peter Albert, Amjad Almahairi, Yasmine Babaei, Nikolay  
 819 Bashlykov, Soumya Batra, Prajjwal Bhargava, Shruti Bhosale, Dan Bikel, Lukas Blecher, Cris-  
 820 tian Canton Ferrer, Moya Chen, Guillem Cucurull, David Esiobu, Jude Fernandes, Jeremy Fu,  
 821 Wenying Fu, Brian Fuller, Cynthia Gao, Vedanuj Goswami, Naman Goyal, Anthony Hartshorn,  
 822 Saghar Hosseini, Rui Hou, Hakan Inan, Marcin Kardas, Viktor Kerkez, Madian Khabsa, Isabel  
 823 Kloumann, Artem Korenev, Punit Singh Koura, Marie-Anne Lachaux, Thibaut Lavril, Jenya Lee,  
 824 Diana Liskovich, Yinghai Lu, Yuning Mao, Xavier Martinet, Todor Mihaylov, Pushkar Mishra,  
 825 Igor Molybog, Yixin Nie, Andrew Poulton, Jeremy Reizenstein, Rashi Rungta, Kalyan Saladi,  
 826 Alan Schelten, Ruan Silva, Eric Michael Smith, Ranjan Subramanian, Xiaoqing Ellen Tan, Binh  
 827 Tang, Ross Taylor, Adina Williams, Jian Xiang Kuan, Puxin Xu, Zheng Yan, Iliyan Zarov, Yuchen  
 828 Zhang, Angela Fan, Melanie Kambadur, Sharan Narang, Aurelien Rodriguez, Robert Stojnic,  
 829 Sergey Edunov, and Thomas Scialom. Llama 2: Open foundation and fine-tuned chat models.  
 830 *arXiv preprint arXiv:2307.09288*, 2023. 8

831

832 Ashish Vaswani, Noam Shazeer, Niki Parmar, Jakob Uszkoreit, Llion Jones, Aidan N Gomez, Łukasz  
 833 Kaiser, and Illia Polosukhin. Attention is all you need. In *NeurIPS*, 2017. 1, 2, 3, 4

834

835 Petar Veličković, Guillem Cucurull, Arantxa Casanova, Adriana Romero, Pietro Liò, and Yoshua  
 836 Bengio. Graph attention networks. In *ICLR*, 2018. 2, 10

837

838 Jianghui Wang, Yang Chen, Xingyu Xie, Cong Fang, and Zhouchen Lin. Task-robust pre-training  
 839 for worst-case downstream adaptation. *Advances in Neural Information Processing Systems*, 36:  
 840 9458–9478, 2023. 8

841

842 Pei Wang and Nuno Vasconcelos. A machine teaching framework for scalable recognition. In *ICCV*,  
 843 2021. 3

844

845 Pei Wang, Kabir Nagrecha, and Nuno Vasconcelos. Gradient-based algorithms for machine teaching.  
 846 In *CVPR*, 2021a. 3

847

848 Xin Wang, Yudong Chen, and Wenwu Zhu. A survey on curriculum learning. *IEEE transactions on  
 849 pattern analysis and machine intelligence*, 44(9):4555–4576, 2021b. 9

850

851 Tong Wei, Hao-Tian Li, Chun-Shu Li, Jiang-Xin Shi, Yu-Feng Li, and Min-Ling Zhang. Vision-  
 852 language models are strong noisy label detectors. In *NeurIPS*, 2024. 10

853

854 Stephen J Wright. Coordinate descent algorithms. *Mathematical programming*, 151(1):3–34, 2015. 7

855

856 Likang Wu, Zhi Zheng, Zhaopeng Qiu, Hao Wang, Hongchao Gu, Tingjia Shen, Chuan Qin, Chen  
 857 Zhu, Hengshu Zhu, Qi Liu, Hui Xiong, and Enhong Chen. A survey on large language models for  
 858 recommendation. *World Wide Web*, 27(5):60, 2024. 2

859

860 Can Xu, Qingfeng Sun, Kai Zheng, Xiubo Geng, Pu Zhao, Jiazhan Feng, Chongyang Tao, Qingwei  
 861 Lin, and Dixin Jiang. WizardLM: Empowering large pre-trained language models to follow  
 862 complex instructions. In *The Twelfth International Conference on Learning Representations*, 2023.  
 863 8

864

865 Antoine Yang, Arsha Nagrani, Paul Hongsuck Seo, Antoine Miech, Jordi Pont-Tuset, Ivan Laptev,  
 866 Josef Sivic, and Cordelia Schmid. Vid2Seq: Large-scale pretraining of a visual language model for  
 867 dense video captioning. In *CVPR*, pp. 10714–10726, 2023. 1

868

869 Greg Yang. Wide feedforward or recurrent neural networks of any architecture are gaussian processes.  
 870 *Advances in Neural Information Processing Systems*, 32, 2019. 2, 5, 6, 25

864 Hongyu Yang, Jinjiao Zhang, Liang Zhang, Xiang Cheng, and Ze Hu. MRAN: Multimodal  
 865 relationship-aware attention network for fake news detection. *Computer Standards & Interfaces*,  
 866 89:103822, 2024. 1

867

868 Haoran You, Chaojian Li, Pengfei Xu, Yonggan Fu, Yue Wang, Xiaohan Chen, Richard G Baraniuk,  
 869 Zhangyang Wang, and Yingyan Lin. Drawing early-bird tickets: Toward more efficient training of  
 870 deep networks. In *International Conference on Learning Representations*, 2020. 2

871 Longhui Yu, Weisen Jiang, Han Shi, Jincheng Yu, Zhengying Liu, Yu Zhang, James T Kwok, Zhenguo  
 872 Li, Adrian Weller, and Weiyang Liu. MetaMath: Bootstrap your own mathematical questions for  
 873 large language models. *arXiv preprint arXiv:2309.12284*, 2023a. 8

874

875 Weichen Yu, Tianyu Pang, Qian Liu, Chao Du, Bingyi Kang, Yan Huang, Min Lin, and Shuicheng  
 876 Yan. Bag of tricks for training data extraction from language models. In *International Conference  
 877 on Machine Learning*, pp. 40306–40320. PMLR, 2023b. 5

878 Chen Zhang, Xiaofeng Cao, Weiyang Liu, Ivor Tsang, and James Kwok. Nonparametric teaching for  
 879 multiple learners. In *NeurIPS*, 2023a. 1, 2, 3, 19, 24, 26

880 Chen Zhang, Xiaofeng Cao, Weiyang Liu, Ivor Tsang, and James Kwok. Nonparametric iterative  
 881 machine teaching. In *ICML*, 2023b. 1, 2, 3, 4, 9, 19, 32

882

883 Chen Zhang, Steven Tin Sui Luo, Jason Chun Lok Li, Yik-Chung Wu, and Ngai Wong. Nonparametric  
 884 teaching of implicit neural representations. In *ICML*, 2024a. 1, 2, 3, 6, 7

885 Chen Zhang, Weixin Bu, Zeyi Ren, Zhengwu Liu, Yik-Chung Wu, and Ngai Wong. Nonparametric  
 886 teaching for graph property learners. In *ICML*, 2025. 1, 2, 3, 6, 9

887

888 Shuoxi Zhang, Hanpeng Liu, Stephen Lin, and Kun He. You only need less attention at each stage in  
 889 vision transformers. In *Proceedings of the IEEE/CVF Conference on Computer Vision and Pattern  
 890 Recognition*, pp. 6057–6066, 2024b. 2

891 Lianmin Zheng, Wei-Lin Chiang, Ying Sheng, Siyuan Zhuang, Zhanghao Wu, Yonghao Zhuang,  
 892 Zi Lin, Zhuohan Li, Dacheng Li, Eric P. Xing, Hao Zhang, Joseph E. Gonzalez, and Ion Stoica.  
 893 Judging LLM-as-a-judge with MT-Bench and chatbot arena. *Advances in Neural Information  
 894 Processing Systems*, 36, 2024a. 8

895

896 Tianyu Zheng, Ge Zhang, Tianhao Shen, Xueling Liu, Bill Yuchen Lin, Jie Fu, Wenhui Chen, and  
 897 Xiang Yue. OpenCodeInterpreter: Integrating code generation with execution and refinement.  
 898 *arXiv preprint arXiv:2402.14658*, 2024b. 8

899

900 Qihuang Zhong, Liang Ding, Juhua Liu, Xuebo Liu, Min Zhang, Bo Du, and Dacheng Tao. Revisiting  
 901 token dropping strategy in efficient bert pretraining. In *Proceedings of the 61st Annual Meeting of  
 902 the Association for Computational Linguistics (Volume 1: Long Papers)*, pp. 10391–10405, 2023.  
 903 2

904

905 Yao Zhou, Arun Reddy Nelakurthi, and Jingrui He. Unlearn what you have learned: Adaptive crowd  
 906 teaching with exponentially decayed memory learners. In *SIGKDD*, 2018. 3

907

908 Xiaojin Zhu. Machine teaching: An inverse problem to machine learning and an approach toward  
 909 optimal education. In *AAAI*, 2015. 1, 3

910

911 Xiaojin Zhu, Adish Singla, Sandra Zilles, and Anna N Rafferty. An overview of machine teaching.  
 912 *arXiv preprint arXiv:1801.05927*, 2018. 1, 3

913

914

915

916

917

# Appendix

918	<b>A Additional Discussions</b>	<b>19</b>
919	A.1 Notation Overview	19
920	A.2 Functional Gradient	19
921	A.3 The Derivation of Importance-adaptive Updates in the Parameter Space.	19
922	A.4 Attention Neural Tangent Kernel (ANTK)	24
923	A.5 AtteNT Algorithm	26
924		
925	<b>B Detailed Proofs</b>	<b>27</b>
926	B.1 Proof of Theorem 3	27
927	B.2 Proof of Proposition 4	27
928		
929	<b>C Experiment Details</b>	<b>31</b>
930	C.1 LLMs Training Setting	31
931	C.2 ViTs Training Setting	31
932		
933	<b>D Additional Experiments</b>	<b>33</b>
934	D.1 Ablation of Sample Ratio	33
935	D.2 Comparison to Established Methods	33
936	D.3 Visualizing NTK Analysis	34
937		
938	<b>E The Use of Large Language Models (LLMs)</b>	<b>35</b>
939		
940		
941		
942		
943		
944		
945		
946		
947		
948		
949		
950		
951		
952		
953		
954		
955		
956		
957		
958		
959		
960		
961		
962		
963		
964		
965		
966		
967		
968		
969		
970		
971		

972 **A ADDITIONAL DISCUSSIONS**  
973974 **A.1 NOTATION OVERVIEW**  
975976 Table 4: Summary of Key Notations.  
977

978 <b>Notation</b>	979 <b>Description</b>
980 $\mathbf{S}_{S \times d}$	981 Matrix containing all feature vectors from the ordered sequence ( $\mathbf{x}_1, \dots, \mathbf{x}_S$ ), with shape $S \times d$
982 $[x_{s,j}]_d^\top$	983 $d$ -dimensional feature vector for the $s$ -th element, with components $x_{s,j}$
983 $\mathbf{x}$	984 Short form for $[x_j]_d$
984 $\mathbf{S}_{(s,:)}$	985 The $s$ -th row of $\mathbf{S}$ , representing the feature vector for the $s$ -th element
985 $\mathbf{S}_{(:,i)}$	986 The $i$ -th column of $\mathbf{S}$ , which represents the $i$ -th feature across all elements)
986 $\mathbf{e}_i$	987 The $i$ -th basis vector, having a value of 1 at the $i$ -th position and 0 elsewhere
988 $\mathcal{S}$	989 Collection of all sequences
989 $\mathbf{y}$	990 Property associated with the sequences, which can be scalar or vector
990 $\mathcal{Y}$	991 Space of sequential properties, represented as $\mathbb{R}$ or $\mathbb{R}^n$
991 $\{a_i\}_m$	992 A set containing $m$ items
992 $\text{diag}(a_1, \dots, a_m)$	993 Diagonal matrix with diagonal entries $a_1, \dots, a_m$
993 $\text{diag}(a; m)$	994 Diagonal matrix with $m$ repeated entries of $a$
994 $\mathbb{N}_S := \{1, \dots, S\}$	995 Set of natural numbers from 1 to $S$
995 $K(\mathbf{S}, \mathbf{S}')$	996 A symmetric and positive definite sequence kernel
996 $\mathcal{H}$	997 Reproducing kernel Hilbert space (RKHS) defined by $K$
997 $f^*$	998 Target mapping from $\mathcal{S}$ to $\mathcal{Y}$
998 $\mathbf{y}_\dagger$	999 Property $f^*(\mathbf{S}_\dagger)$ corresponding to the sequence $\mathbf{S}_\dagger$

1000 **A.2 FUNCTIONAL GRADIENT**  
1001

1002 [Zhang et al., 2023b;a](#) present the chain rule for functional gradients, which is detailed in  
1003 Lemma 5 ([Gelfand & Silverman, 2000](#)), and utilize the Fréchet derivative to calculate the derivative  
1004 of the evaluation functional in RKHS, as shown in Lemma 6 ([Coleman, 2012](#)).

1005 **Lemma 5.** (*Chain rule for functional gradients*) For differentiable functions  $G(F) : \mathbb{R} \mapsto \mathbb{R}$  that  
1006 depend on functionals  $F(f) : \mathcal{H} \mapsto \mathbb{R}$ , the chain rule is given by

$$1008 \nabla_f G(F(f)) = \frac{\partial G(F(f))}{\partial F(f)} \cdot \nabla_f F(f). \quad (22)$$

1010 **Lemma 6.** The gradient of the evaluation functional at the feature  $\mathbf{x}$ , denoted as  
1011  $E_{\mathbf{x}}(f) = f(\mathbf{x}) : \mathcal{H} \mapsto \mathbb{R}$ , is given by  $\nabla_f E_{\mathbf{x}}(f) = K(\mathbf{x}, \cdot)$ , where  $K(\mathbf{x}, \mathbf{x}') : \mathbb{R}^d \times \mathbb{R}^d \mapsto \mathbb{R}$   
1012 represents a feature-based kernel.

1013 **A.3 THE DERIVATION OF IMPORTANCE-ADAPTIVE UPDATES IN THE PARAMETER SPACE.**  
1014

1015 Before providing the detailed derivation, we begin by showing visualizations of general single-head  
1016 attention learners. Figure 2a depicts a multi-output self-attention learner, Figure 2b presents a  
1017 multi-output masked self-attention learner, and Figure 2c illustrates a multi-output cross-attention  
1018 learner. The formulations for the masked self-attention and cross-attention learners are presented in  
1019 Equation 23.

$$1021 \text{Masked Self-Attention: } f_\theta(\mathbf{S}) = \text{softmax} \left( \frac{\mathcal{Q}(\mathbf{S})\mathcal{K}(\mathbf{S})^\top}{\sqrt{d}} + \mathbf{M} \right) \mathcal{V}(\mathbf{S}) \\ 1022 \text{Cross-Attention: } f_\theta(\mathbf{S}, \mathbf{S}') = \text{softmax} \left( \frac{\mathcal{Q}(\mathbf{S})\mathcal{K}(\mathbf{S}')^\top}{\sqrt{d}} \right) \mathcal{V}(\mathbf{S}'), \quad (23)$$

1023 where  $\mathbf{M} \in \mathbb{R}^{S \times S}$  is a a is a strictly upper triangular matrix, with zeros on and below the diagonal and  
1024  $-\infty$  in every element above the diagonal.

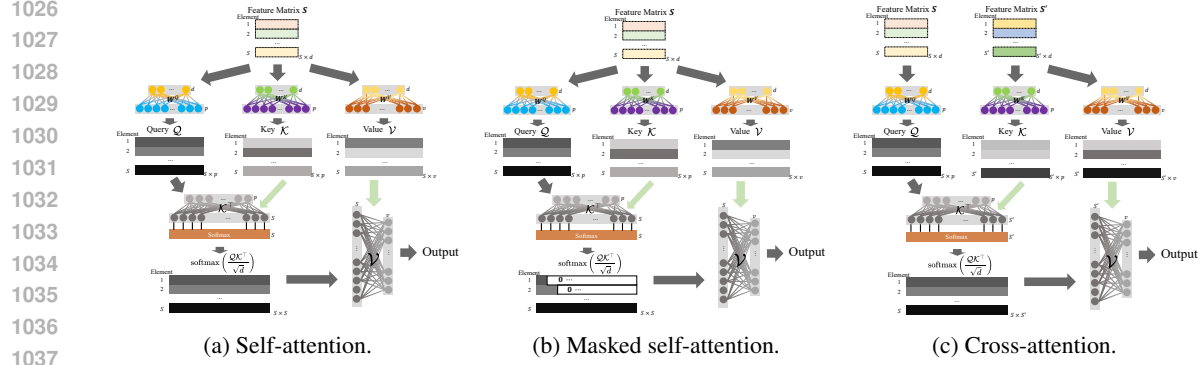


Figure 2: An illustration of the workflow for different multi-output attention learners, with input sequence  $\mathbf{S}$  and  $\mathbf{S}'$  (in the case of cross-attention).

Consider the derivative of an ANN with  $v = 1$ , meaning that each component of the output  $f_{\theta^t}(\mathbf{S})_{(j,:)}$  is a scalar:

$$\frac{\partial f_{\theta}(\mathbf{S})}{\partial \theta} = \left[ \frac{\partial f_{\theta}(\mathbf{S})}{\partial \mathbf{W}^V}, \frac{\partial f_{\theta}(\mathbf{S})}{\partial \mathbf{W}^Q}, \dots, \frac{\partial f_{\theta}(\mathbf{S})}{\partial \mathbf{W}_{(:,1)}^Q}, \frac{\partial f_{\theta}(\mathbf{S})}{\partial \mathbf{W}_{(:,1)}^K}, \dots, \frac{\partial f_{\theta}(\mathbf{S})}{\partial \mathbf{W}_{(:,1)}^K} \right]. \quad (24)$$

By applying the chain rule, we can compute the derivative of  $f_{\theta}(\mathbf{S})$  with respect to the weight  $\mathbf{W}^V$  in the value matrix  $\mathcal{V}(\mathbf{S})$ .

$$\begin{aligned} \frac{\partial f_{\theta}(\mathbf{S})}{\partial \mathbf{W}^V} &= \frac{\partial \text{softmax} \left( \frac{\mathcal{Q}(\mathbf{S})\mathcal{K}(\mathbf{S})^{\top}}{\sqrt{d}} \right) \mathcal{V}(\mathbf{S})}{\partial \mathbf{W}^V} \\ &= \frac{\partial \text{softmax} \left( \frac{\mathbf{S}\mathbf{W}^Q \mathbf{W}^K \mathbf{S}^{\top}}{\sqrt{d}} \right) \mathbf{S}\mathbf{W}^V}{\partial \mathbf{W}^V} \\ &= \text{softmax} \left( \frac{\mathbf{S}\mathbf{W}^Q \mathbf{W}^K \mathbf{S}^{\top}}{\sqrt{d}} \right) \mathbf{S} \\ &= \text{softmax} \left( \frac{\mathcal{Q}\mathcal{K}^{\top}}{\sqrt{d}} \right) \mathbf{S} \\ &= \left[ \frac{\exp \left( \mathcal{Q}_{(i,:)}\mathcal{K}^{\top}/\sqrt{d} \right)}{\mathbf{1}^{\top} \exp \left( \mathcal{Q}_{(i,:)}\mathcal{K}^{\top}/\sqrt{d} \right)} \right]_S \mathbf{S}, \end{aligned} \quad (25)$$

where  $\exp(\cdot)$  denotes the row-wise exponential operator. The case of  $v \geq 2$  represents a multi-dimensional extension, which involves more complex notation but can be derived in a similar manner.

1080 The derivative of  $f_\theta(\mathbf{S})$  with respect to the query weight matrix is more intricate. For  $i \in \mathbb{N}_p$ ,  
 1081

$$\begin{aligned}
 \frac{\partial f_\theta(\mathbf{S})}{\partial \mathbf{W}_{(:,i)}^Q} &= \frac{\partial \text{softmax} \left( \frac{\mathcal{Q}(\mathbf{S}) \mathcal{K}(\mathbf{S})^\top}{\sqrt{d}} \right) \mathcal{V}(\mathbf{S})}{\partial \mathbf{W}_{(:,i)}^Q} \\
 &= \frac{\partial \text{softmax} \left( \frac{\mathbf{S} \mathbf{W}^Q \mathbf{W}^{K^\top} \mathbf{S}^\top}{\sqrt{d}} \right) \mathbf{S} \mathbf{W}^V}{\partial \mathbf{W}_{(:,i)}^Q} \\
 &= \frac{\partial \text{softmax} \left( \frac{\mathbf{S} \mathbf{W}^Q \mathbf{e}_i \mathbf{e}_i^\top \mathbf{W}^{K^\top} \mathbf{S}^\top}{\sqrt{d}} \right) \mathbf{S} \mathbf{W}^V}{\partial \mathbf{W}_{(:,i)}^Q} \\
 &= \left[ \begin{array}{c} \frac{\partial \text{softmax} \left( \frac{\mathbf{S}_{(1,:)} \mathbf{W}_{(:,i)}^Q \mathbf{W}_{(:,i)}^{K^\top} \mathbf{S}^\top}{\sqrt{d}} \right) \mathbf{S} \mathbf{W}^V}{\partial \mathbf{W}_{(:,i)}^Q} \\ \vdots \\ \frac{\partial \text{softmax} \left( \frac{\mathbf{S}_{(S,:)} \mathbf{W}_{(:,i)}^Q \mathbf{W}_{(:,i)}^{K^\top} \mathbf{S}^\top}{\sqrt{d}} \right) \mathbf{S} \mathbf{W}^V}{\partial \mathbf{W}_{(:,i)}^Q} \end{array} \right] \\
 &= \left[ \begin{array}{c} \frac{\partial \frac{\mathbf{S}_{(1,:)} \mathbf{W}_{(:,i)}^Q \mathbf{W}_{(:,i)}^{K^\top} \mathbf{S}^\top}{\sqrt{d}}}{\partial \mathbf{W}_{(:,i)}^Q} \frac{\partial \text{softmax} \left( \frac{\mathbf{S}_{(1,:)} \mathbf{W}_{(:,i)}^Q \mathbf{W}_{(:,i)}^{K^\top} \mathbf{S}^\top}{\sqrt{d}} \right)}{\partial \frac{\mathbf{S}_{(1,:)} \mathbf{W}_{(:,i)}^Q \mathbf{W}_{(:,i)}^{K^\top} \mathbf{S}^\top}{\sqrt{d}}} \mathbf{S} \mathbf{W}^V \\ \vdots \\ \frac{\partial \frac{\mathbf{S}_{(S,:)} \mathbf{W}_{(:,i)}^Q \mathbf{W}_{(:,i)}^{K^\top} \mathbf{S}^\top}{\sqrt{d}}}{\partial \mathbf{W}_{(:,i)}^Q} \frac{\partial \text{softmax} \left( \frac{\mathbf{S}_{(S,:)} \mathbf{W}_{(:,i)}^Q \mathbf{W}_{(:,i)}^{K^\top} \mathbf{S}^\top}{\sqrt{d}} \right)}{\partial \frac{\mathbf{S}_{(S,:)} \mathbf{W}_{(:,i)}^Q \mathbf{W}_{(:,i)}^{K^\top} \mathbf{S}^\top}{\sqrt{d}}} \mathbf{S} \mathbf{W}^V \end{array} \right]. \tag{26}
 \end{aligned}$$

1112 Let's examine this row by row. For the  $j$ -th row ( $j \in \mathbb{N}_S$ ) of Equation 26, it expressed as:

$$\begin{aligned}
 &\frac{\partial \frac{\mathbf{S}_{(j,:)} \mathbf{W}_{(:,i)}^Q \mathbf{W}_{(:,i)}^{K^\top} \mathbf{S}^\top}{\sqrt{d}}}{\partial \mathbf{W}_{(:,i)}^Q} \frac{\partial \text{softmax} \left( \frac{\mathbf{S}_{(j,:)} \mathbf{W}_{(:,i)}^Q \mathbf{W}_{(:,i)}^{K^\top} \mathbf{S}^\top}{\sqrt{d}} \right)}{\partial \frac{\mathbf{S}_{(j,:)} \mathbf{W}_{(:,i)}^Q \mathbf{W}_{(:,i)}^{K^\top} \mathbf{S}^\top}{\sqrt{d}}} \mathbf{S} \mathbf{W}^V \\
 &= \mathbf{S}_{(j,:)} \cdot \frac{1}{\sqrt{d}} \mathbf{W}_{(:,i)}^{K^\top} \mathbf{S}^\top \frac{\partial \text{softmax} \left( \frac{\mathbf{S}_{(j,:)} \mathbf{W}_{(:,i)}^Q \mathbf{W}_{(:,i)}^{K^\top} \mathbf{S}^\top}{\sqrt{d}} \right)}{\partial \frac{\mathbf{S}_{(j,:)} \mathbf{W}_{(:,i)}^Q \mathbf{W}_{(:,i)}^{K^\top} \mathbf{S}^\top}{\sqrt{d}}} \mathbf{S} \mathbf{W}^V \\
 &= \mathbf{S}_{(j,:)} \cdot \frac{1}{\sqrt{d}} \mathbf{W}_{(:,i)}^{K^\top} \mathbf{S}^\top \frac{\partial \left( \frac{\exp(d^{-1/2} \mathbf{S}_{(j,:)} \mathbf{W}_{(:,i)}^Q \mathbf{W}_{(:,i)}^{K^\top} \mathbf{S}^\top)}{\mathbf{1}^\top \exp(d^{-1/2} \mathbf{S}_{(j,:)} \mathbf{W}_{(:,i)}^Q \mathbf{W}_{(:,i)}^{K^\top} \mathbf{S}^\top)} \right)}{\partial d^{-1/2} \mathbf{S}_{(j,:)} \mathbf{W}_{(:,i)}^Q \mathbf{W}_{(:,i)}^{K^\top} \mathbf{S}^\top} \mathbf{S} \mathbf{W}^V \\
 &= \mathbf{S}_{(j,:)} \cdot \left( \frac{1}{\sqrt{d}} \mathbf{W}_{(:,i)}^{K^\top} \mathbf{S}^\top \text{diag} \left( \text{softmax} \left( \mathbf{S}_{(j,:)} \mathbf{W}_{(:,i)}^Q \mathbf{W}_{(:,i)}^{K^\top} \mathbf{S}^\top / \sqrt{d} \right) \right) \mathbf{S} \mathbf{W}^V \right. \\
 &\quad \left. - \frac{1}{\sqrt{d}} \mathbf{W}_{(:,i)}^{K^\top} \mathbf{S}^\top \left( \text{softmax} \left( \mathbf{S}_{(j,:)} \mathbf{W}_{(:,i)}^Q \mathbf{W}_{(:,i)}^{K^\top} \mathbf{S}^\top / \sqrt{d} \right) \right)^\top \text{softmax} \left( \mathbf{S}_{(j,:)} \mathbf{W}_{(:,i)}^Q \mathbf{W}_{(:,i)}^{K^\top} \mathbf{S}^\top / \sqrt{d} \right) \mathbf{S} \mathbf{W}^V \right). \tag{27}
 \end{aligned}$$

1134 The right-hand side of Equation 27 can be rewritten as  
 1135

1136  
 1137  
 1138  
 1139

$$\begin{aligned}
 & \underbrace{\mathbf{S}_{(j,:)} \cdot \left( \underbrace{d^{-1/2} \mathbf{W}_{(:,i)}^K}^{1 \times d} \underbrace{\mathbf{S}^\top}^{1 \times d} \underbrace{\text{diag} \left( \text{softmax} \left( \underbrace{\mathbf{S}_{(j,:)} \mathbf{W}_{(:,i)}^Q \mathbf{W}_{(:,i)}^{K^\top} \mathbf{S}^\top}_{S \times S} / \sqrt{d} \right) \right)}_{d \times S} \mathbf{S}_{(j,:)} \mathbf{W}_{(:,i)}^V}_{\text{size: } 1 \times d} \\
 & - \underbrace{d^{-1/2} \mathbf{W}_{(:,i)}^K}^{1 \times 1} \underbrace{\mathbf{S}^\top}_{1 \times d} \underbrace{\left( \text{softmax} \left( \underbrace{\mathbf{S}_{(j,:)} \mathbf{W}_{(:,i)}^Q \mathbf{W}_{(:,i)}^{K^\top} \mathbf{S}^\top}_{S \times 1} / \sqrt{d} \right) \right)^\top}_{S \times 1} \underbrace{\text{softmax} \left( \underbrace{\mathbf{S}_{(j,:)} \mathbf{W}_{(:,i)}^Q \mathbf{W}_{(:,i)}^{K^\top} \mathbf{S}^\top}_{1 \times S} / \sqrt{d} \right)}_{1 \times S} \mathbf{S}_{(j,:)} \mathbf{W}_{(:,i)}^V \\
 & = \underbrace{\mathbf{S}_{(j,:)} \cdot \left( \underbrace{d^{-1/2} \mathcal{K}_{(:,i)}^\top}_{1 \times 1} \underbrace{\text{diag} \left( \text{softmax} \left( \underbrace{\mathcal{Q}_{(j,i)} \mathcal{K}_{(:,i)}^\top}_{S \times S} / \sqrt{d} \right) \right)}_{1 \times S} \mathcal{V}}_{1 \times d} \\
 & - \underbrace{d^{-1/2} \mathcal{K}_{(:,i)}^\top}_{1 \times 1} \underbrace{\left( \text{softmax} \left( \underbrace{\mathcal{Q}_{(j,i)} \mathcal{K}_{(:,i)}^\top}_{S \times 1} / \sqrt{d} \right) \right)^\top}_{S \times 1} \underbrace{\text{softmax} \left( \underbrace{\mathcal{Q}_{(j,i)} \mathcal{K}_{(:,i)}^\top}_{1 \times S} / \sqrt{d} \right)}_{1 \times S} \mathcal{V} \\
 & = d^{-1/2} \underbrace{\mathbf{S}_{(j,:)} \cdot \left( \underbrace{\mathcal{K}_{(:,i)}^\top}_{1 \times d} \underbrace{\text{diag} \left( \text{softmax} \left( \mathcal{Q}_{(j,i)} \mathcal{K}_{(:,i)}^\top / \sqrt{d} \right) \right)}_{S \times S} \mathcal{V} - \underbrace{\mathcal{K}_{(:,i)}^\top}_{1 \times d} \underbrace{\left( \text{softmax} \left( \mathcal{Q}_{(j,i)} \mathcal{K}_{(:,i)}^\top / \sqrt{d} \right) \right)^\top}_{S \times S} \underbrace{\text{softmax} \left( \mathcal{Q}_{(j,i)} \mathcal{K}_{(:,i)}^\top / \sqrt{d} \right)}_{S \times 1} \mathcal{V}}_{1 \times 1}. \tag{28}
 \end{aligned}$$

1165 By combining Equation 26, 27 and 28, we derive  
 1166

1167  
 1168  
 1169  
 1170

$$\begin{aligned}
 & \frac{\partial f_\theta(\mathbf{S})}{\partial \mathbf{W}_{(:,i)}^Q} \\
 & = \left[ \begin{array}{c} d^{-1/2} \underbrace{\mathbf{S}_{(1,:)} \cdot \left( \underbrace{\mathcal{K}_{(:,i)}^\top}_{1 \times d} \underbrace{\text{diag} \left( \text{softmax} \left( \mathcal{Q}_{(1,i)} \mathcal{K}_{(:,i)}^\top / \sqrt{d} \right) \right)}_{S \times S} \mathcal{V} - \underbrace{\mathcal{K}_{(:,i)}^\top}_{1 \times d} \underbrace{\left( \text{softmax} \left( \mathcal{Q}_{(1,i)} \mathcal{K}_{(:,i)}^\top / \sqrt{d} \right) \right)^\top}_{S \times S} \underbrace{\text{softmax} \left( \mathcal{Q}_{(1,i)} \mathcal{K}_{(:,i)}^\top / \sqrt{d} \right)}_{S \times 1} \mathcal{V} \right)}_{1 \times 1} \\ \dots \\ d^{-1/2} \underbrace{\mathbf{S}_{(S,:)} \cdot \left( \underbrace{\mathcal{K}_{(:,i)}^\top}_{1 \times d} \underbrace{\text{diag} \left( \text{softmax} \left( \mathcal{Q}_{(S,i)} \mathcal{K}_{(:,i)}^\top / \sqrt{d} \right) \right)}_{S \times S} \mathcal{V} - \underbrace{\mathcal{K}_{(:,i)}^\top}_{1 \times d} \underbrace{\left( \text{softmax} \left( \mathcal{Q}_{(S,i)} \mathcal{K}_{(:,i)}^\top / \sqrt{d} \right) \right)^\top}_{S \times S} \underbrace{\text{softmax} \left( \mathcal{Q}_{(S,i)} \mathcal{K}_{(:,i)}^\top / \sqrt{d} \right)}_{S \times 1} \mathcal{V} \right)}_{S \times d} \end{array} \right]_{S \times d} \\
 & = \left[ d^{-1/2} \mathbf{S}_{(j,:)} \cdot \left( \mathcal{K}_{(:,i)}^\top \text{diag} \left( \text{softmax} \left( \mathcal{Q}_{(j,i)} \mathcal{K}_{(:,i)}^\top / \sqrt{d} \right) \right) \mathcal{V} - \mathcal{K}_{(:,i)}^\top \left( \text{softmax} \left( \mathcal{Q}_{(j,i)} \mathcal{K}_{(:,i)}^\top / \sqrt{d} \right) \right)^\top \underbrace{\text{softmax} \left( \mathcal{Q}_{(j,i)} \mathcal{K}_{(:,i)}^\top / \sqrt{d} \right)}_{S \times 1} \mathcal{V} \right] \right]_{S \times d} \\
 & = \text{diag} \left( \mathcal{K}_{(:,i)}^\top \text{diag} \left( \text{softmax} \left( \mathcal{Q}_{(1,i)} \mathcal{K}_{(:,i)}^\top / \sqrt{d} \right) \right) \mathcal{V} - \mathcal{K}_{(:,i)}^\top \left( \text{softmax} \left( \mathcal{Q}_{(1,i)} \mathcal{K}_{(:,i)}^\top / \sqrt{d} \right) \right)^\top \underbrace{\text{softmax} \left( \mathcal{Q}_{(1,i)} \mathcal{K}_{(:,i)}^\top / \sqrt{d} \right)}_{S \times 1} \mathcal{V}, \right. \\
 & \quad \left. \dots, \mathcal{K}_{(:,i)}^\top \text{diag} \left( \text{softmax} \left( \mathcal{Q}_{(S,i)} \mathcal{K}_{(:,i)}^\top / \sqrt{d} \right) \right) \mathcal{V} - \mathcal{K}_{(:,i)}^\top \left( \text{softmax} \left( \mathcal{Q}_{(S,i)} \mathcal{K}_{(:,i)}^\top / \sqrt{d} \right) \right)^\top \underbrace{\text{softmax} \left( \mathcal{Q}_{(S,i)} \mathcal{K}_{(:,i)}^\top / \sqrt{d} \right)}_{S \times 1} \mathcal{V} \right) \mathbf{S} / \sqrt{d}. \tag{29}
 \end{aligned}$$

1188 The derivative of  $f_\theta(\mathbf{S})$  with respect to the key weight matrix is derived in a manner similar to that of  
 1189 the query weight matrix. For  $i \in \mathbb{N}_p$ ,  
 1190

$$\begin{aligned}
 & \frac{\partial f_\theta(\mathbf{S})}{\partial \mathbf{W}_{(:,i)}^K} \\
 &= \frac{\partial \text{softmax}\left(\frac{\mathcal{Q}(\mathbf{S})\mathcal{K}(\mathbf{S})^\top}{\sqrt{d}}\right) \mathcal{V}(\mathbf{S})}{\partial \mathbf{W}_{(:,i)}^K} \\
 &= \frac{\partial \text{softmax}\left(\frac{\mathbf{S}\mathbf{W}^Q \mathbf{W}^{K^\top} \mathbf{S}^\top}{\sqrt{d}}\right) \mathbf{S}\mathbf{W}^V}{\partial \mathbf{W}_{(:,i)}^K} \\
 &= \frac{\partial \text{softmax}\left(\frac{\mathbf{S}\mathbf{W}^Q (\mathbf{W}^K \mathbf{e}_i \mathbf{e}_i^\top)^\top \mathbf{S}^\top}{\sqrt{d}}\right) \mathbf{S}\mathbf{W}^V}{\partial \mathbf{W}_{(:,i)}^K} \\
 &= \left[ \frac{\partial \text{softmax}\left(\frac{\mathbf{S}_{(1,:)} \mathbf{W}_{(:,i)}^Q \mathbf{W}_{(:,i)}^{K^\top} \mathbf{S}^\top}{\sqrt{d}}\right) \mathbf{S}\mathbf{W}^V}{\partial \mathbf{W}_{(:,i)}^K} \right. \\
 &\quad \left. \cdots \right. \\
 &\quad \left. \frac{\partial \text{softmax}\left(\frac{\mathbf{S}_{(S,:)} \mathbf{W}_{(:,i)}^Q \mathbf{W}_{(:,i)}^{K^\top} \mathbf{S}^\top}{\sqrt{d}}\right) \mathbf{S}\mathbf{W}^V}{\partial \mathbf{W}_{(:,i)}^K} \right] \\
 &= \left[ \frac{\frac{\partial \mathbf{S}_{(1,:)} \mathbf{W}_{(:,i)}^Q \mathbf{W}_{(:,i)}^{K^\top} \mathbf{S}^\top}{\sqrt{d}} \partial \text{softmax}\left(\frac{\mathbf{S}_{(1,:)} \mathbf{W}_{(:,i)}^Q \mathbf{W}_{(:,i)}^{K^\top} \mathbf{S}^\top}{\sqrt{d}}\right)}{\partial \mathbf{W}_{(:,i)}^K} \mathbf{S}\mathbf{W}^V \right. \\
 &\quad \left. \cdots \right. \\
 &\quad \left. \frac{\frac{\partial \mathbf{S}_{(S,:)} \mathbf{W}_{(:,i)}^Q \mathbf{W}_{(:,i)}^{K^\top} \mathbf{S}^\top}{\sqrt{d}} \partial \text{softmax}\left(\frac{\mathbf{S}_{(S,:)} \mathbf{W}_{(:,i)}^Q \mathbf{W}_{(:,i)}^{K^\top} \mathbf{S}^\top}{\sqrt{d}}\right)}{\partial \mathbf{W}_{(:,i)}^K} \mathbf{S}\mathbf{W}^V \right]. \tag{30}
 \end{aligned}$$

1221 Similarly, let's examine it row by row. For the  $j$ -th row ( $j \in \mathbb{N}_S$ ) of Equation 30, it is  
 1222

$$\begin{aligned}
 & \frac{\partial \frac{\mathbf{S}_{(j,:)} \mathbf{W}_{(:,i)}^Q \mathbf{W}_{(:,i)}^{K^\top} \mathbf{S}^\top}{\sqrt{d}} \partial \text{softmax}\left(\frac{\mathbf{S}_{(j,:)} \mathbf{W}_{(:,i)}^Q \mathbf{W}_{(:,i)}^{K^\top} \mathbf{S}^\top}{\sqrt{d}}\right)}{\partial \mathbf{W}_{(:,i)}^K} \mathbf{S}\mathbf{W}^V \\
 &= \mathbf{S}_{(j,:)} \cdot \frac{1}{\sqrt{d}} \mathbf{W}_{(:,i)}^Q \mathbf{S}^\top \frac{\partial \text{softmax}\left(\frac{\mathbf{S}_{(j,:)} \mathbf{W}_{(:,i)}^Q \mathbf{W}_{(:,i)}^{K^\top} \mathbf{S}^\top}{\sqrt{d}}\right)}{\partial \frac{\mathbf{S}_{(j,:)} \mathbf{W}_{(:,i)}^Q \mathbf{W}_{(:,i)}^{K^\top} \mathbf{S}^\top}{\sqrt{d}}} \mathbf{S}\mathbf{W}^V \\
 &= \mathbf{S}_{(j,:)} \cdot \frac{1}{\sqrt{d}} \mathbf{W}_{(:,i)}^Q \mathbf{S}^\top \frac{\partial \left( \frac{\exp(d^{-1/2} \mathbf{S}_{(j,:)} \mathbf{W}_{(:,i)}^Q \mathbf{W}_{(:,i)}^{K^\top} \mathbf{S}^\top)}{\mathbf{1}^\top \exp(d^{-1/2} \mathbf{S}_{(j,:)} \mathbf{W}_{(:,i)}^Q \mathbf{W}_{(:,i)}^{K^\top} \mathbf{S}^\top)} \right)}{\partial d^{-1/2} \mathbf{S}_{(j,:)} \mathbf{W}_{(:,i)}^Q \mathbf{W}_{(:,i)}^{K^\top} \mathbf{S}^\top} \mathbf{S}\mathbf{W}^V \\
 &= \mathbf{S}_{(j,:)} \cdot \left( \frac{1}{\sqrt{d}} \mathbf{W}_{(:,i)}^Q \mathbf{S}^\top \text{diag}\left(\text{softmax}(\mathbf{S}_{(j,:)} \mathbf{W}_{(:,i)}^Q \mathbf{W}_{(:,i)}^{K^\top} \mathbf{S}^\top / \sqrt{d})\right) \mathbf{S}\mathbf{W}^V \right. \\
 &\quad \left. - \frac{1}{\sqrt{d}} \mathbf{W}_{(:,i)}^Q \mathbf{S}^\top \left( \text{softmax}(\mathbf{S}_{(j,:)} \mathbf{W}_{(:,i)}^Q \mathbf{W}_{(:,i)}^{K^\top} \mathbf{S}^\top / \sqrt{d}) \right)^\top \text{softmax}(\mathbf{S}_{(j,:)} \mathbf{W}_{(:,i)}^Q \mathbf{W}_{(:,i)}^{K^\top} \mathbf{S}^\top / \sqrt{d}) \mathbf{S}\mathbf{W}^V \right). \tag{31}
 \end{aligned}$$

1242 The right-hand side of Equation 31 can be simplified to:  
1243

$$\begin{aligned}
1244 & \underbrace{\mathbf{S}_{(j,:)} \cdot \left( \underbrace{d^{-1/2} \mathbf{W}_{(:,i)}^Q}^{1 \times d} \underbrace{\mathbf{S}^\top}^{d \times S} \underbrace{\text{diag} \left( \text{softmax} \left( \underbrace{\mathbf{S}_{(j,:)} \mathbf{W}_{(:,i)}^Q \mathbf{W}_{(:,i)}^{K^\top} \mathbf{S}^\top}_{S \times S} / \sqrt{d} \right) \right)}_{1 \times d} \underbrace{\mathbf{S}}_{S \times d} \underbrace{\mathbf{W}^V}_{d \times 1} \right)}_{\text{size: } 1 \times d} \\
1245 & - \underbrace{d^{-1/2} \mathbf{W}_{(:,i)}^Q \mathbf{S}^\top}_{1 \times d} \underbrace{\left( \text{softmax} \left( \underbrace{\mathbf{S}_{(j,:)} \mathbf{W}_{(:,i)}^Q \mathbf{W}_{(:,i)}^{K^\top} \mathbf{S}^\top}_{S \times 1} / \sqrt{d} \right) \right)^\top}_{S \times 1} \underbrace{\text{softmax} \left( \underbrace{\mathbf{S}_{(j,:)} \mathbf{W}_{(:,i)}^Q \mathbf{W}_{(:,i)}^{K^\top} \mathbf{S}^\top}_{1 \times S} / \sqrt{d} \right)}_{1 \times S} \underbrace{\mathbf{S}}_{S \times d} \underbrace{\mathbf{W}^V}_{d \times 1} \\
1246 & = \underbrace{\mathbf{S}_{(j,:)} \cdot \left( \underbrace{d^{-1/2} \mathcal{Q}_{(:,i)}^\top}_{1 \times d} \underbrace{\text{diag} \left( \text{softmax} \left( \underbrace{\mathcal{Q}_{(j,i)} \mathcal{K}_{(:,i)}^\top}_{S \times S} / \sqrt{d} \right) \right)}_{1 \times S} \underbrace{\mathcal{V}}_{S \times 1} \right)}_{\text{size: } 1 \times d} \\
1247 & - \underbrace{d^{-1/2} \mathcal{Q}_{(:,i)}^\top}_{1 \times d} \underbrace{\left( \text{softmax} \left( \underbrace{\mathcal{Q}_{(j,i)} \mathcal{K}_{(:,i)}^\top}_{S \times 1} / \sqrt{d} \right) \right)^\top}_{S \times 1} \underbrace{\text{softmax} \left( \underbrace{\mathcal{Q}_{(j,i)} \mathcal{K}_{(:,i)}^\top}_{1 \times S} / \sqrt{d} \right)}_{1 \times S} \underbrace{\mathcal{V}}_{S \times 1} \\
1248 & = \underbrace{d^{-1/2} \mathbf{S}_{(j,:)} \left( \underbrace{\mathcal{Q}_{(:,i)}^\top \text{diag} \left( \text{softmax} \left( \mathcal{Q}_{(j,i)} \mathcal{K}_{(:,i)}^\top / \sqrt{d} \right) \right)}_{1 \times S} \underbrace{\mathcal{V}}_{S \times 1} - \underbrace{\mathcal{Q}_{(:,i)}^\top \left( \text{softmax} \left( \mathcal{Q}_{(j,i)} \mathcal{K}_{(:,i)}^\top / \sqrt{d} \right) \right)^\top \text{softmax} \left( \mathcal{Q}_{(j,i)} \mathcal{K}_{(:,i)}^\top / \sqrt{d} \right)}_{S \times S} \underbrace{\mathcal{V}}_{S \times 1} \right)}_{1 \times 1}. \tag{32}
\end{aligned}$$

1249 By merging Equation 30, 31 and 32, we get:  
1250

$$\begin{aligned}
1251 & \frac{\partial f_\theta(\mathbf{S})}{\partial \mathbf{W}_{(:,i)}^K} \\
1252 & = \left[ \begin{array}{c} \underbrace{d^{-1/2} \mathbf{S}_{(1,:)} \cdot \left( \underbrace{\mathcal{Q}_{(:,i)}^\top \text{diag} \left( \text{softmax} \left( \mathcal{Q}_{(1,i)} \mathcal{K}_{(:,i)}^\top / \sqrt{d} \right) \right)}_{1 \times S} \underbrace{\mathcal{V}}_{S \times 1} - \underbrace{\mathcal{Q}_{(:,i)}^\top \left( \text{softmax} \left( \mathcal{Q}_{(1,i)} \mathcal{K}_{(:,i)}^\top / \sqrt{d} \right) \right)^\top \text{softmax} \left( \mathcal{Q}_{(1,i)} \mathcal{K}_{(:,i)}^\top / \sqrt{d} \right)}_{1 \times 1} \underbrace{\mathcal{V}}_{S \times 1} \right) \\ \dots \\ \underbrace{d^{-1/2} \mathbf{S}_{(S,:)} \cdot \left( \underbrace{\mathcal{Q}_{(:,i)}^\top \text{diag} \left( \text{softmax} \left( \mathcal{Q}_{(S,i)} \mathcal{K}_{(:,i)}^\top / \sqrt{d} \right) \right)}_{1 \times S} \underbrace{\mathcal{V}}_{S \times 1} - \underbrace{\mathcal{Q}_{(:,i)}^\top \left( \text{softmax} \left( \mathcal{Q}_{(S,i)} \mathcal{K}_{(:,i)}^\top / \sqrt{d} \right) \right)^\top \text{softmax} \left( \mathcal{Q}_{(S,i)} \mathcal{K}_{(:,i)}^\top / \sqrt{d} \right)}_{1 \times 1} \underbrace{\mathcal{V}}_{S \times 1} \right)_{S \times d} \end{array} \right]_{S \times d} \\
1253 & = \left[ \begin{array}{c} \left[ d^{-1/2} \mathbf{S}_{(j,:)} \cdot \left( \mathcal{Q}_{(:,i)}^\top \text{diag} \left( \text{softmax} \left( \mathcal{Q}_{(j,i)} \mathcal{K}_{(:,i)}^\top / \sqrt{d} \right) \right) \mathcal{V} - \mathcal{Q}_{(:,i)}^\top \left( \text{softmax} \left( \mathcal{Q}_{(j,i)} \mathcal{K}_{(:,i)}^\top / \sqrt{d} \right) \right)^\top \text{softmax} \left( \mathcal{Q}_{(j,i)} \mathcal{K}_{(:,i)}^\top / \sqrt{d} \right) \mathcal{V} \right] \\ \dots \\ \mathcal{Q}_{(:,i)}^\top \text{diag} \left( \text{softmax} \left( \mathcal{Q}_{(1,i)} \mathcal{K}_{(:,i)}^\top / \sqrt{d} \right) \right) \mathcal{V} - \mathcal{Q}_{(:,i)}^\top \left( \text{softmax} \left( \mathcal{Q}_{(1,i)} \mathcal{K}_{(:,i)}^\top / \sqrt{d} \right) \right)^\top \text{softmax} \left( \mathcal{Q}_{(1,i)} \mathcal{K}_{(:,i)}^\top / \sqrt{d} \right) \mathcal{V} \end{array} \right]_{S \times d} \\
1254 & = \text{diag} \left( \mathcal{Q}_{(:,i)}^\top \text{diag} \left( \text{softmax} \left( \mathcal{Q}_{(1,i)} \mathcal{K}_{(:,i)}^\top / \sqrt{d} \right) \right) \mathcal{V} - \mathcal{Q}_{(:,i)}^\top \left( \text{softmax} \left( \mathcal{Q}_{(1,i)} \mathcal{K}_{(:,i)}^\top / \sqrt{d} \right) \right)^\top \text{softmax} \left( \mathcal{Q}_{(1,i)} \mathcal{K}_{(:,i)}^\top / \sqrt{d} \right) \mathcal{V}, \right. \\
1255 & \quad \left. \dots, \mathcal{Q}_{(:,i)}^\top \text{diag} \left( \text{softmax} \left( \mathcal{Q}_{(S,i)} \mathcal{K}_{(:,i)}^\top / \sqrt{d} \right) \right) \mathcal{V} - \mathcal{Q}_{(:,i)}^\top \left( \text{softmax} \left( \mathcal{Q}_{(S,i)} \mathcal{K}_{(:,i)}^\top / \sqrt{d} \right) \right)^\top \text{softmax} \left( \mathcal{Q}_{(S,i)} \mathcal{K}_{(:,i)}^\top / \sqrt{d} \right) \mathcal{V} \right) \mathbf{S} / \sqrt{d}. \tag{33}
\end{aligned}$$

1256 From Equations 25, 29, and 33, it can be observed that the ANN gradient for a single sequence  
1257 resembles that for a batch of feature vector inputs, as the gradient can be decomposed for each  
1258 element. This demonstrates the parallelization-friendly nature of the attention mechanism from a  
1259 gradient perspective.  
1260

1261 These results can be directly extended to the case where each component of the output  $f_{\theta^t}(\mathbf{S})_{(j,:)}$  is a  
1262 vector, by considering a multi-dimensional setting (Zhang et al., 2023a). The extension to multi-head  
1263 cases can be done by broadcasting, which involves repeating the derivation in parallel as many times  
1264 as there are heads.  
1265

#### A.4 ATTENTION NEURAL TANGENT KERNEL (ANTK)

1266 By incorporating the parameter evolution (i.e., Equation 7)

$$\frac{\partial \theta^t}{\partial t} = -\frac{\eta}{NS} \left[ \frac{\partial \mathcal{L}(f_{\theta^t}(\mathbf{S}_1), \mathbf{y}_1)}{\partial f_{\theta^t}(\mathbf{S}_1)}, \dots, \frac{\partial \mathcal{L}(f_{\theta^t}(\mathbf{S}_N), \mathbf{y}_N)}{\partial f_{\theta^t}(\mathbf{S}_N)} \right] \cdot \left[ \frac{\partial f_{\theta^t}(\mathbf{S}_i)}{\partial \theta^t} \right]_N. \tag{34}$$

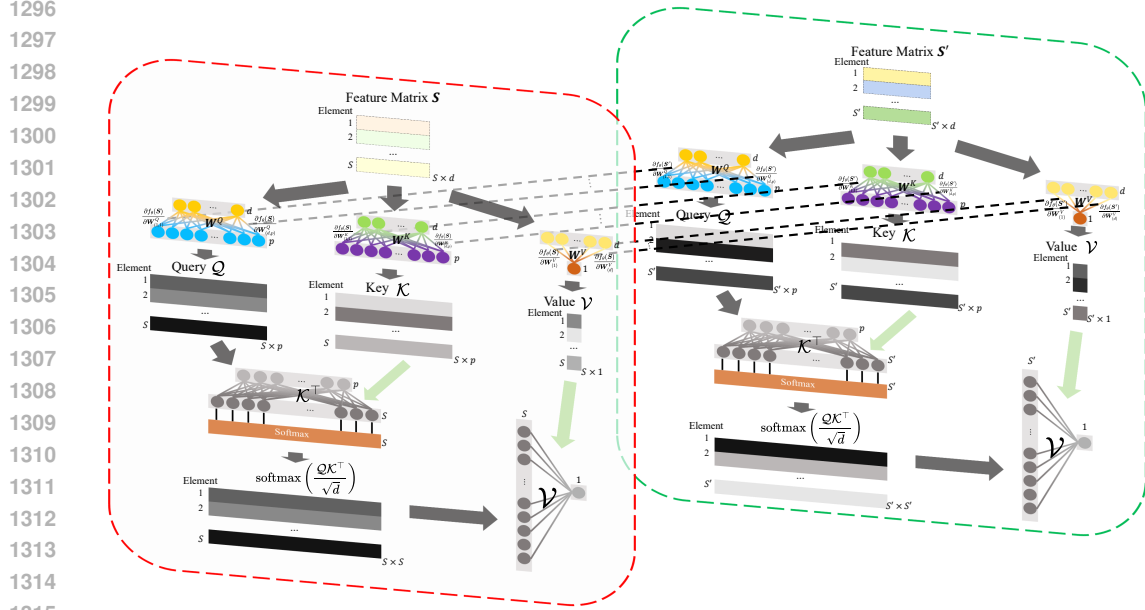


Figure 3: Graphical depiction of the ANTK computation process:  $K_\theta(\mathbf{S}_S, \mathbf{S}'_{S'}) = \left\langle \frac{\partial f_\theta(\mathbf{S})}{\partial \theta}, \frac{\partial f_\theta(\mathbf{S}')}{\partial \theta} \right\rangle = \left[ \frac{\partial f_\theta(\mathbf{S}_{(i,:)})}{\partial \mathbf{W}_{(1)}^V} \frac{\partial f_\theta(\mathbf{S}')_{(j,:)}}{\partial \mathbf{W}_{(1)}^V} + \dots + \frac{\partial f_\theta(\mathbf{S}_{(i,:)})}{\partial \mathbf{W}_{(d)}^V} \frac{\partial f_\theta(\mathbf{S}')_{(j,:)}}{\partial \mathbf{W}_{(d)}^V} + \frac{\partial f_\theta(\mathbf{S}_{(i,:)})}{\partial \mathbf{W}_{(1,1)}^Q} \frac{\partial f_\theta(\mathbf{S}')_{(j,:)}}{\partial \mathbf{W}_{(1,1)}^Q} + \dots + \frac{\partial f_\theta(\mathbf{S}_{(i,:)})}{\partial \mathbf{W}_{(d,p)}^Q} \frac{\partial f_\theta(\mathbf{S}')_{(j,:)}}{\partial \mathbf{W}_{(d,p)}^Q} + \frac{\partial f_\theta(\mathbf{S}_{(i,:)})}{\partial \mathbf{W}_{(1,1)}^K} \frac{\partial f_\theta(\mathbf{S}')_{(j,:)}}{\partial \mathbf{W}_{(1,1)}^K} + \dots + \frac{\partial f_\theta(\mathbf{S}_{(i,:)})}{\partial \mathbf{W}_{(d,p)}^K} \frac{\partial f_\theta(\mathbf{S}')_{(j,:)}}{\partial \mathbf{W}_{(d,p)}^K} \right]_{S \times S'; i \in \mathbb{N}_S, j \in \mathbb{N}_{S'}}.$

into the first-order approximation term (\*) of Equation 14, we derive

$$\begin{aligned}
 (*) &= \left\langle \frac{\partial f_{\theta^t}(\cdot)}{\partial \theta^t}, -\frac{\eta}{NS} \left[ \frac{\partial \mathcal{L}(f_{\theta^t}(\mathbf{S}_1), \mathbf{y}_1)}{\partial f_{\theta^t}(\mathbf{S}_1)}, \dots, \frac{\partial \mathcal{L}(f_{\theta^t}(\mathbf{S}_N), \mathbf{y}_N)}{\partial f_{\theta^t}(\mathbf{S}_N)} \right] \cdot \left[ \frac{\partial f_{\theta^t}(\mathbf{S}_i)}{\partial \theta^t} \right]_N \right\rangle \\
 &= -\frac{\eta}{NS} \left[ \frac{\partial \mathcal{L}(f_{\theta^t}(\mathbf{S}_1), \mathbf{y}_1)}{\partial f_{\theta^t}(\mathbf{S}_1)}, \dots, \frac{\partial \mathcal{L}(f_{\theta^t}(\mathbf{S}_N), \mathbf{y}_N)}{\partial f_{\theta^t}(\mathbf{S}_N)} \right] \cdot \left\langle \frac{\partial f_{\theta^t}(\cdot)}{\partial \theta^t}, \left[ \frac{\partial f_{\theta^t}(\mathbf{S}_i)}{\partial \theta^t} \right]_N \right\rangle \\
 &= -\frac{\eta}{NS} \left[ \frac{\partial \mathcal{L}(f_{\theta^t}(\mathbf{S}_1), \mathbf{y}_1)}{\partial f_{\theta^t}(\mathbf{S}_1)}, \dots, \frac{\partial \mathcal{L}(f_{\theta^t}(\mathbf{S}_N), \mathbf{y}_N)}{\partial f_{\theta^t}(\mathbf{S}_N)} \right] \cdot \left[ \left\langle \frac{\partial f_{\theta^t}(\cdot)}{\partial \theta^t}, \frac{\partial f_{\theta^t}(\mathbf{S}_i)}{\partial \theta^t} \right\rangle \right]_N \\
 &= -\frac{\eta}{NS} \left[ \frac{\partial \mathcal{L}(f_{\theta^t}(\mathbf{S}_1), \mathbf{y}_1)}{\partial f_{\theta^t}(\mathbf{S}_1)}, \dots, \frac{\partial \mathcal{L}(f_{\theta^t}(\mathbf{S}_N), \mathbf{y}_N)}{\partial f_{\theta^t}(\mathbf{S}_N)} \right] \cdot [K_{\theta^t}(\mathbf{S}_i, \cdot)]_N, \tag{35}
 \end{aligned}$$

which leads to Equation 15 expressed as

$$\frac{\partial f_{\theta^t}}{\partial t} = -\frac{\eta}{NS} \left[ \frac{\partial \mathcal{L}(f_{\theta^t}(\mathbf{S}_1), \mathbf{y}_1)}{\partial f_{\theta^t}(\mathbf{S}_1)}, \dots, \frac{\partial \mathcal{L}(f_{\theta^t}(\mathbf{S}_N), \mathbf{y}_N)}{\partial f_{\theta^t}(\mathbf{S}_N)} \right] \cdot [K_{\theta^t}(\mathbf{S}_i, \cdot)]_N + o\left(\frac{\partial \theta^t}{\partial t}\right), \tag{36}$$

where the symmetric and positive definite  $K_{\theta^t}(\mathbf{S}_i, \cdot) := \left\langle \frac{\partial f_{\theta^t}(\mathbf{S}_i)}{\partial \theta^t}, \frac{\partial f_{\theta^t}(\cdot)}{\partial \theta^t} \right\rangle$  is called the attention neural tangent kernel (ANTK) (Jacot et al., 2018; Yang, 2019; Hron et al., 2020). Specifically, ANTK for  $\mathbf{S}_{(i,:)}$  and  $\mathbf{S}'_{(j,:)}$  is a scalar  $K(\mathbf{S}_{(i,:)}, \mathbf{S}'_{(j,:)}) = \left\langle \frac{\partial f_{\theta^t}(\mathbf{S}_{(i,:)})}{\partial \theta^t}, \frac{\partial f_{\theta^t}(\mathbf{S}'_{(j,:)})}{\partial \theta^t} \right\rangle$ . Figure 3 illustrates the ANTK computation process, where typically, the length of all training sequences is standardized to the maximum length. In simple terms, examining a model’s behavior by focusing on the model itself, rather than its parameters, often involves the use of kernel functions.

The quantity  $\frac{\partial f_{\theta^t}(\cdot)}{\partial \theta^t}$ , which represents the partial derivative of the ANN with respect to its parameters and appears in  $K_{\theta^t}(\mathbf{S}_i, \cdot) = \left\langle \frac{\partial f_{\theta^t}(\mathbf{S}_i)}{\partial \theta^t}, \frac{\partial f_{\theta^t}(\cdot)}{\partial \theta^t} \right\rangle$ , is determined by both the network architecture and the specific parameters  $\theta^t$ , but it is independent of the input sequences. In contrast, the term  $\frac{\partial f_{\theta^t}(\mathbf{S}_i)}{\partial \theta^t}$  depends not only on the ANN structure and specific  $\theta^t$ , but also on the input sequence  $\mathbf{S}$ . When the input for  $\frac{\partial f_{\theta^t}(\mathbf{S}_i)}{\partial \theta^t}$  is unspecified, the ANTK simplifies to a general form  $K_{\theta^t}(\cdot, \cdot)$ .

1350 However, when a specific sequence  $S_j$  is provided as the input to  $\frac{\partial f_{\theta^t}(\cdot)}{\partial \theta^t}$ , the ANTK becomes a  
 1351 matrix defined as  $K_{\theta^t}(S_i, S_j) = \left\langle \frac{\partial f_{\theta^t}(S_i)}{\partial \theta^t}, \frac{\partial f_{\theta^t}(S_j)}{\partial \theta^t} \right\rangle$ . This formulation aligns with the vector-  
 1352 valued kernel used in functional gradient descent (Zhang et al., 2023a). When the input sequence  
 1353  $S_i$  is specified, one argument of  $K_{\theta^t}$  is fixed, leading the ANN to update along  $K_{\theta^t}(S_i, \cdot)$ , with  
 1354 the magnitude of the update determined by  $\frac{\partial f_{\theta^t}(S_i)}{\partial \theta^t}$ . This process reflects the core mechanism of  
 1355 functional gradient descent. In summary, the ANTK and the canonical vector-valued kernel share  
 1356 a consistent mathematical framework and exhibit similar effects on the evolution of the associated  
 1357 ANN. Additionally, Theorem 3 establishes the asymptotic relationship between the ANTK and the  
 1358 canonical kernel used in functional gradient descent.  
 1359

1360 **A.5 ATTENT ALGORITHM**

1361 **Algorithm 1** AtteNT Algorithm

1362 **Input:** Target mapping  $f^*$  realized by a dense set of sequence-property pairs, initial ANN  $f_{\theta^0}$ , the  
 1363 size of selected training set  $m \leq N$ , small constant  $\epsilon > 0$  and maximal iteration number  $T$

1364 Set  $f_{\theta^t} \leftarrow f_{\theta^0}$ ,  $t = 0$

1365 **while**  $t \leq T$  and  $\|[f_{\theta^t}(S_i) - f^*(S_i)]_N\|_{\mathcal{F}} \geq \epsilon$  **do**

1366   **The teacher** selects  $m$  teaching sequences:

1367   /\* Sequences associated with the  $m$  largest  $\|f_{\theta^t}(S_i) - f^*(S_i)\|_2$  \*/  
 1368    $\{S_i\}_m^* = \arg \max_{\{S_i\}_m \subseteq \{S_i\}_N} \|[f_{\theta^t}(S_i) - f^*(S_i)]_m\|_{\mathcal{F}}$

1369   Provide  $\{S_i\}_m^*$  to the attention learner

1370   **The learner** updates  $f_{\theta^t}$  based on received  $\{S_i\}_m^*$ :

1371   // Parameter-based gradient descent

1372    $\theta^t \leftarrow \theta^t - \frac{\eta}{mS} \sum_{S_i \in \{S_i\}_m^*} \sum_{j=1}^S \nabla_{\theta} \mathcal{L}(f_{\theta^t}(S_i)_{(j,:)}, f^*(S_i)_{(j,:)})$

1373   Set  $t \leftarrow t + 1$

1374 **end**

1375

1376

1377

1378

1379

1380

1381

1382

1383

1384

1385

1386

1387

1388

1389

1390

1391

1392

1393

1394

1395

1396

1397

1398

1399

1400

1401

1402

1403

1404 **B DETAILED PROOFS**  
14051406 **B.1 PROOF OF THEOREM 3**  
14071408 By examining the evolution of an ANN through changes in its parameters and from a high-level  
1409 perspective within the function space, we obtain.  
1410

1411  
1412 
$$-\frac{\eta}{NS} \left[ \frac{\partial \mathcal{L}(f_{\theta^t}(\mathbf{S}_1), \mathbf{y}_1)}{\partial f_{\theta^t}(\mathbf{S}_1)}, \dots, \frac{\partial \mathcal{L}(f_{\theta^t}(\mathbf{S}_N), \mathbf{y}_N)}{\partial f_{\theta^t}(\mathbf{S}_N)} \right] [K(\mathbf{S}_i, \cdot)]_N$$
  
1413  
1414 
$$= -\frac{\eta}{NS} \left[ \frac{\partial \mathcal{L}(f_{\theta^t}(\mathbf{S}_1), \mathbf{y}_1)}{\partial f_{\theta^t}(\mathbf{S}_1)}, \dots, \frac{\partial \mathcal{L}(f_{\theta^t}(\mathbf{S}_N), \mathbf{y}_N)}{\partial f_{\theta^t}(\mathbf{S}_N)} \right] \cdot \left[ \left\langle \frac{\partial f_{\theta^t}(\mathbf{S}_i)}{\partial \theta^t}, \frac{\partial f_{\theta^t}(\cdot)}{\partial \theta^t} \right\rangle \right]_N + o\left(\frac{\partial \theta^t}{\partial t}\right). \quad (37)$$
  
1415  
1416  
1417

1418 Upon reorganizing, we derive  
1419

1420  
1421 
$$-\frac{\eta}{NS} \left[ \frac{\partial \mathcal{L}(f_{\theta^t}(\mathbf{S}_1), \mathbf{y}_1)}{\partial f_{\theta^t}(\mathbf{S}_1)}, \dots, \frac{\partial \mathcal{L}(f_{\theta^t}(\mathbf{S}_N), \mathbf{y}_N)}{\partial f_{\theta^t}(\mathbf{S}_N)} \right] \cdot [K(\mathbf{S}_i, \cdot) - K_{\theta^t}(\mathbf{S}_i, \cdot)]_N = o\left(\frac{\partial \theta^t}{\partial t}\right). \quad (38)$$
  
1422  
1423

1424 By integrating the parameter evolution  
1425

1426  
1427 
$$\frac{\partial \theta^t}{\partial t} = -\eta \frac{\partial \mathcal{L}}{\partial \theta^t} = -\frac{\eta}{NS} \left[ \frac{\partial \mathcal{L}(f_{\theta^t}(\mathbf{S}_1), \mathbf{y}_1)}{\partial f_{\theta^t}(\mathbf{S}_1)}, \dots, \frac{\partial \mathcal{L}(f_{\theta^t}(\mathbf{S}_N), \mathbf{y}_N)}{\partial f_{\theta^t}(\mathbf{S}_N)} \right] \cdot \left[ \frac{\partial f_{\theta^t}(\mathbf{S}_i)}{\partial \theta^t} \right]_N \quad (39)$$
  
1428  
1429

1430 into the remainder, we get  
1431

1432  
1433 
$$-\frac{\eta}{NS} \left[ \frac{\partial \mathcal{L}(f_{\theta^t}(\mathbf{S}_1), \mathbf{y}_1)}{\partial f_{\theta^t}(\mathbf{S}_1)}, \dots, \frac{\partial \mathcal{L}(f_{\theta^t}(\mathbf{S}_N), \mathbf{y}_N)}{\partial f_{\theta^t}(\mathbf{S}_N)} \right] \cdot [K(\mathbf{S}_i, \cdot) - K_{\theta^t}(\mathbf{S}_i, \cdot)]_N$$
  
1434  
1435 
$$= o\left(-\frac{\eta}{NS} \left[ \frac{\partial \mathcal{L}(f_{\theta^t}(\mathbf{S}_1), \mathbf{y}_1)}{\partial f_{\theta^t}(\mathbf{S}_1)}, \dots, \frac{\partial \mathcal{L}(f_{\theta^t}(\mathbf{S}_N), \mathbf{y}_N)}{\partial f_{\theta^t}(\mathbf{S}_N)} \right] \cdot \left[ \frac{\partial f_{\theta^t}(\mathbf{S}_i)}{\partial \theta^t} \right]_N\right). \quad (40)$$
  
1436  
1437

1438 When training an ANN with a convex loss  $\mathcal{L}$ , which is convex in terms of  $f_\theta$  but not necessarily in  
1439 terms of  $\theta$ , the following limit holds for the vector:  $\lim_{t \rightarrow \infty} \left[ \frac{\partial \mathcal{L}(f_{\theta^t}(\mathbf{S}_1), \mathbf{y}_1)}{\partial f_{\theta^t}(\mathbf{S}_1)}, \dots, \frac{\partial \mathcal{L}(f_{\theta^t}(\mathbf{S}_N), \mathbf{y}_N)}{\partial f_{\theta^t}(\mathbf{S}_N)} \right] =$   
1440 **0**. Since the right-hand side of this equation is a higher-order infinitesimal relative to the left,  
1441 maintaining this equality results in the conclusion that  
1442

1443 
$$\lim_{t \rightarrow \infty} [K(\mathbf{S}_i, \cdot) - K_{\theta^t}(\mathbf{S}_i, \cdot)]_N = \mathbf{0}. \quad (41)$$
  
1444  
1445

1446 This suggests that for each training point, *i.e.*, input sequence  $\mathbf{S} \in \{\mathbf{S}_i\}_N$ , ANTK converges  
1447 pointwise to the canonical kernel.  
1448  $\blacksquare$   
14491450 **B.2 PROOF OF PROPOSITION 4**  
14511452 Referring to the definition of the Fréchet derivative in Definition 2, the convexity of  $\mathcal{L}$  implies that  
1453

1454  
1455 
$$\frac{\partial \mathcal{L}}{\partial t} \leq \underbrace{\left\langle \frac{\partial \mathcal{L}}{\partial f_{\theta^{t+1}}}, \frac{f_{\theta^t}}{\partial t} \right\rangle}_{\Upsilon} \quad (42)$$
  
1456  
1457

1458 By computing the Fréchet derivative of  $\frac{\partial \mathcal{L}}{\partial f_{\theta^{t+1}}}$  and the evolution of  $f_{\theta^t}$ , the term on the right-hand  
 1459 side,  $\Upsilon$ , can be expressed as  
 1460

$$\begin{aligned}
 \Upsilon &= \langle \mathcal{G}^{t+1}, -\eta \mathcal{G}^t \rangle_{\mathcal{H}} \\
 &= -\frac{\eta}{N^2 S^2} \left\langle \left[ \frac{\partial \mathcal{L}(f_{\theta^{t+1}}(\mathbf{S}_1), \mathbf{y}_1)}{\partial f_{\theta^{t+1}}(\mathbf{S}_1)}, \dots, \frac{\partial \mathcal{L}(f_{\theta^{t+1}}(\mathbf{S}_N), \mathbf{y}_N)}{\partial f_{\theta^{t+1}}(\mathbf{S}_N)} \right] \cdot [K_{\mathbf{S}_i}]_N, \right. \\
 &\quad \left. [K_{\mathbf{S}_i}]_N^\top \cdot \left[ \frac{\partial \mathcal{L}(f_{\theta^t}(\mathbf{S}_1), \mathbf{y}_1)}{\partial f_{\theta^t}(\mathbf{S}_1)}, \dots, \frac{\partial \mathcal{L}(f_{\theta^t}(\mathbf{S}_N), \mathbf{y}_N)}{\partial f_{\theta^t}(\mathbf{S}_N)} \right]^\top \right\rangle_{\mathcal{H}} \\
 &= -\frac{\eta}{N^2 S^2} \left[ \frac{\partial \mathcal{L}(f_{\theta^{t+1}}(\mathbf{S}_1), \mathbf{y}_1)}{\partial f_{\theta^{t+1}}(\mathbf{S}_1)}, \dots, \frac{\partial \mathcal{L}(f_{\theta^{t+1}}(\mathbf{S}_N), \mathbf{y}_N)}{\partial f_{\theta^{t+1}}(\mathbf{S}_N)} \right] \cdot \langle [K_{\mathbf{S}_i}]_N, [K_{\mathbf{S}_i}]_N^\top \rangle_{\mathcal{H}} \\
 &\quad \cdot \left[ \frac{\partial \mathcal{L}(f_{\theta^t}(\mathbf{S}_1), \mathbf{y}_1)}{\partial f_{\theta^t}(\mathbf{S}_1)}, \dots, \frac{\partial \mathcal{L}(f_{\theta^t}(\mathbf{S}_N), \mathbf{y}_N)}{\partial f_{\theta^t}(\mathbf{S}_N)} \right]^\top \\
 &= -\frac{\eta}{NS} \left[ \frac{\partial \mathcal{L}(f_{\theta^{t+1}}(\mathbf{S}_1), \mathbf{y}_1)}{\partial f_{\theta^{t+1}}(\mathbf{S}_1)}, \dots, \frac{\partial \mathcal{L}(f_{\theta^{t+1}}(\mathbf{S}_N), \mathbf{y}_N)}{\partial f_{\theta^{t+1}}(\mathbf{S}_N)} \right] \bar{\mathbf{K}} \left[ \frac{\partial \mathcal{L}(f_{\theta^t}(\mathbf{S}_1), \mathbf{y}_1)}{\partial f_{\theta^t}(\mathbf{S}_1)}, \dots, \frac{\partial \mathcal{L}(f_{\theta^t}(\mathbf{S}_N), \mathbf{y}_N)}{\partial f_{\theta^t}(\mathbf{S}_N)} \right]^\top, \tag{43}
 \end{aligned}$$

1475 where  $\bar{\mathbf{K}} = \mathbf{K}/(NS)$ , and  $\mathbf{K}$  is an  $NS \times NS$  symmetric, positive definite block matrix with elements  
 1476  $K(\mathbf{S}_i, \mathbf{S}_j)$  positioned in the  $i$ -th row and  $j$ -th column block. For convenience, we use a simplified  
 1477 column vector notation  $[\partial_{f_{\theta^{\square}}} \mathcal{L}(f_{\theta^{\square}}; \mathbf{S}_i)]_N := [\partial_{f_{\theta^{\square}}} \mathcal{L}(f_{\theta^{\square}}; \mathbf{S}_1), \dots, \partial_{f_{\theta^{\square}}} \mathcal{L}(f_{\theta^{\square}}; \mathbf{S}_N)]^\top$  with  
 1478  $\partial_{f_{\theta^{\square}}} \mathcal{L}(f_{\theta^{\square}}; \mathbf{S}_i) := \frac{\partial \mathcal{L}(f_{\theta^{\square}}(\mathbf{S}_i), \mathbf{y}_i)}{\partial f_{\theta^{\square}}(\mathbf{S}_i)}$ . The last term in Equation 43 can then be rewritten as

$$\begin{aligned}
 &-\frac{\eta}{NS} [\partial_{f_{\theta^t}} \mathcal{L}(f_{\theta^t}; \mathbf{S}_i)]_N^\top \bar{\mathbf{K}} [\partial_{f_{\theta^{t+1}}} \mathcal{L}(f_{\theta^{t+1}}; \mathbf{S}_i)]_N \\
 &= -\frac{\eta}{NS} [\partial_{f_{\theta^t}} \mathcal{L}(f_{\theta^t}; \mathbf{S}_i)]_N^\top \bar{\mathbf{K}} \left( [\partial_{f_{\theta^{t+1}}} \mathcal{L}(f_{\theta^{t+1}}; \mathbf{S}_i)]_N + [\partial_{f_{\theta^t}} \mathcal{L}(f_{\theta^t}; \mathbf{S}_i)]_N - [\partial_{f_{\theta^t}} \mathcal{L}(f_{\theta^t}; \mathbf{S}_i)]_N \right) \\
 &= -\frac{\eta}{NS} [\partial_{f_{\theta^t}} \mathcal{L}(f_{\theta^t}; \mathbf{S}_i)]_N^\top \bar{\mathbf{K}} [\partial_{f_{\theta^t}} \mathcal{L}(f_{\theta^t}; \mathbf{S}_i)]_N \\
 &\quad - \frac{\eta}{NS} [\partial_{f_{\theta^t}} \mathcal{L}(f_{\theta^t}; \mathbf{S}_i)]_N^\top \bar{\mathbf{K}} \left( [\partial_{f_{\theta^{t+1}}} \mathcal{L}(f_{\theta^{t+1}}; \mathbf{S}_i)]_N - [\partial_{f_{\theta^t}} \mathcal{L}(f_{\theta^t}; \mathbf{S}_i)]_N \right) \\
 &= -\frac{\eta}{NS} [\partial_{f_{\theta^t}} \mathcal{L}(f_{\theta^t}; \mathbf{S}_i)]_N^\top \bar{\mathbf{K}} [\partial_{f_{\theta^t}} \mathcal{L}(f_{\theta^t}; \mathbf{S}_i)]_N \\
 &\quad + \frac{\eta}{NS} \left( [\partial_{f_{\theta^{t+1}}} \mathcal{L}(f_{\theta^{t+1}}; \mathbf{S}_i)]_N^\top - [\partial_{f_{\theta^t}} \mathcal{L}(f_{\theta^t}; \mathbf{S}_i)]_N^\top - [\partial_{f_{\theta^{t+1}}} \mathcal{L}(f_{\theta^{t+1}}; \mathbf{S}_i)]_N^\top \right) \\
 &\quad \cdot \bar{\mathbf{K}} \cdot \left( [\partial_{f_{\theta^{t+1}}} \mathcal{L}(f_{\theta^{t+1}}; \mathbf{S}_i)]_N - [\partial_{f_{\theta^t}} \mathcal{L}(f_{\theta^t}; \mathbf{S}_i)]_N \right). \tag{44}
 \end{aligned}$$

1494 The last term in Equation 44 above can be expanded to

$$\begin{aligned}
 &\frac{\eta}{NS} \left( [\partial_{f_{\theta^{t+1}}} \mathcal{L}(f_{\theta^{t+1}}; \mathbf{S}_i)]_N^\top - [\partial_{f_{\theta^t}} \mathcal{L}(f_{\theta^t}; \mathbf{S}_i)]_N^\top - [\partial_{f_{\theta^{t+1}}} \mathcal{L}(f_{\theta^{t+1}}; \mathbf{S}_i)]_N^\top \right) \\
 &\quad \cdot \bar{\mathbf{K}} \left( [\partial_{f_{\theta^{t+1}}} \mathcal{L}(f_{\theta^{t+1}}; \mathbf{S}_i)]_N - [\partial_{f_{\theta^t}} \mathcal{L}(f_{\theta^t}; \mathbf{S}_i)]_N \right) \\
 &= \frac{\eta}{NS} \left( [\partial_{f_{\theta^{t+1}}} \mathcal{L}(f_{\theta^{t+1}}; \mathbf{S}_i)]_N - [\partial_{f_{\theta^t}} \mathcal{L}(f_{\theta^t}; \mathbf{S}_i)]_N \right)^\top \bar{\mathbf{K}} \left( [\partial_{f_{\theta^{t+1}}} \mathcal{L}(f_{\theta^{t+1}}; \mathbf{S}_i)]_N - [\partial_{f_{\theta^t}} \mathcal{L}(f_{\theta^t}; \mathbf{S}_i)]_N \right) \\
 &\quad - \frac{\eta}{NS} [\partial_{f_{\theta^{t+1}}} \mathcal{L}(f_{\theta^{t+1}}; \mathbf{S}_i)]_N^\top \bar{\mathbf{K}} \left( [\partial_{f_{\theta^{t+1}}} \mathcal{L}(f_{\theta^{t+1}}; \mathbf{S}_i)]_N - [\partial_{f_{\theta^t}} \mathcal{L}(f_{\theta^t}; \mathbf{S}_i)]_N \right) \\
 &= \frac{\eta}{NS} [\partial_{f_{\theta^{t+1}}} \mathcal{L}(f_{\theta^{t+1}}; \mathbf{S}_i) - \partial_{f_{\theta^t}} \mathcal{L}(f_{\theta^t}; \mathbf{S}_i)]_N^\top \bar{\mathbf{K}} [\partial_{f_{\theta^{t+1}}} \mathcal{L}(f_{\theta^{t+1}}; \mathbf{S}_i) - \partial_{f_{\theta^t}} \mathcal{L}(f_{\theta^t}; \mathbf{S}_i)]_N \\
 &\quad - \frac{\eta}{NS} \left( [\partial_{f_{\theta^{t+1}}} \mathcal{L}(f_{\theta^{t+1}}; \mathbf{S}_i)]_N - \frac{1}{2} [\partial_{f_{\theta^t}} \mathcal{L}(f_{\theta^t}; \mathbf{S}_i)]_N \right)^\top \bar{\mathbf{K}} \left( [\partial_{f_{\theta^{t+1}}} \mathcal{L}(f_{\theta^{t+1}}; \mathbf{S}_i)]_N - \frac{1}{2} [\partial_{f_{\theta^t}} \mathcal{L}(f_{\theta^t}; \mathbf{S}_i)]_N \right) \\
 &\quad + \frac{\eta}{4NS} [\partial_{f_{\theta^t}} \mathcal{L}(f_{\theta^t}; \mathbf{S}_i)]_N^\top \bar{\mathbf{K}} [\partial_{f_{\theta^t}} \mathcal{L}(f_{\theta^t}; \mathbf{S}_i)]_N. \tag{45}
 \end{aligned}$$

1509 Given that  $\bar{\mathbf{K}}$  is positive definite, it follows that

$$\frac{\eta}{NS} \left( [\partial_{f_{\theta^{t+1}}} \mathcal{L}(f_{\theta^{t+1}}; \mathbf{S}_i)]_N - \frac{1}{2} [\partial_{f_{\theta^t}} \mathcal{L}(f_{\theta^t}; \mathbf{S}_i)]_N \right)^\top \bar{\mathbf{K}} \left( [\partial_{f_{\theta^{t+1}}} \mathcal{L}(f_{\theta^{t+1}}; \mathbf{S}_i)]_N - \frac{1}{2} [\partial_{f_{\theta^t}} \mathcal{L}(f_{\theta^t}; \mathbf{S}_i)]_N \right)$$

1512 is a non-negative term. Therefore, by merging Equations 43, 44, and 45, we derive  
 1513

$$\begin{aligned}
 \Upsilon &\leq -\frac{3\eta}{4NS} \underbrace{[\partial_{f_{\theta^t}} \mathcal{L}(f_{\theta^t}; \mathbf{S}_i)]_N^\top \bar{\mathbf{K}} [\partial_{f_{\theta^t}} \mathcal{L}(f_{\theta^t}; \mathbf{S}_i)]_N}_\Phi \\
 &\quad + \frac{\eta}{NS} \underbrace{[\partial_{f_{\theta^{t+1}}} \mathcal{L}(f_{\theta^{t+1}}; \mathbf{S}_i) - \partial_{f_{\theta^t}} \mathcal{L}(f_{\theta^t}; \mathbf{S}_i)]_N^\top \bar{\mathbf{K}} [\partial_{f_{\theta^{t+1}}} \mathcal{L}(f_{\theta^{t+1}}; \mathbf{S}_i) - \partial_{f_{\theta^t}} \mathcal{L}(f_{\theta^t}; \mathbf{S}_i)]_N}_\Psi.
 \end{aligned} \tag{46}$$

1521 Based on the definition of the evaluation functional and the assumption that  $\mathcal{L}$  is Lipschitz smooth  
 1522 with a constant  $\tau > 0$ , the term  $\Psi$  in the final part of Equation 46 is bounded above as follows:  
 1523

$$\begin{aligned}
 \Psi &= [\partial_{f_{\theta^{t+1}}} \mathcal{L}(f_{\theta^{t+1}}; \mathbf{S}_i) - \partial_{f_{\theta^t}} \mathcal{L}(f_{\theta^t}; \mathbf{S}_i)]_N^\top \bar{\mathbf{K}} [\partial_{f_{\theta^{t+1}}} \mathcal{L}(f_{\theta^{t+1}}; \mathbf{S}_i) - \partial_{f_{\theta^t}} \mathcal{L}(f_{\theta^t}; \mathbf{S}_i)]_N \\
 &= \left[ E_{\mathbf{S}_i} \left( \frac{\partial \mathcal{L}(f_{\theta^{t+1}})}{\partial f_{\theta^{t+1}}} - \frac{\partial \mathcal{L}(f_{\theta^t})}{\partial f_{\theta^t}} \right) \right]_N^\top \bar{\mathbf{K}} \left[ E_{\mathbf{S}_i} \left( \frac{\partial \mathcal{L}(f_{\theta^{t+1}})}{\partial f_{\theta^{t+1}}} - \frac{\partial \mathcal{L}(f_{\theta^t})}{\partial f_{\theta^t}} \right) \right]_N \\
 &\leq \tau^2 [E_{\mathbf{S}_i} (f_{\theta^{t+1}} - f_{\theta^t})]_N^\top \bar{\mathbf{K}} [E_{\mathbf{S}_i} (f_{\theta^{t+1}} - f_{\theta^t})]_N \\
 &= \tau^2 \langle (f_{\theta^{t+1}} - f_{\theta^t}), [K_{\mathbf{S}_i}]_N^\top \rangle_{\mathcal{H}} \cdot \bar{\mathbf{K}} \cdot \langle [K_{\mathbf{S}_i}]_N, (f_{\theta^{t+1}} - f_{\theta^t}) \rangle_{\mathcal{H}} \\
 &= \eta^2 \tau^2 \cdot [\partial_{f_{\theta^t}} \mathcal{L}(f_{\theta^t}; \mathbf{S}_i)]_N^\top \frac{\langle [K_{\mathbf{S}_i}]_N, [K_{\mathbf{S}_i}]_N^\top \rangle_{\mathcal{H}}}{NS} \cdot \bar{\mathbf{K}} \cdot \frac{\langle [K_{\mathbf{S}_i}]_N, [K_{\mathbf{S}_i}]_N^\top \rangle_{\mathcal{H}}}{NS} \cdot [\partial_{f_{\theta^t}} \mathcal{L}(f_{\theta^t}; \mathbf{S}_i)]_N.
 \end{aligned} \tag{47}$$

1534 Given that the canonical kernel is bounded above by a constant  $\gamma > 0$ , we have  
 1535

$$\langle [K_{\mathbf{S}_i}]_N, [K_{\mathbf{S}_i}]_N^\top \rangle_{\mathcal{H}} \leq \gamma \langle \mathbf{1}_{NS}, \mathbf{1}_{NS}^\top \rangle,$$

1538 and

$$\bar{\mathbf{K}} \leq \frac{\gamma}{NS} \langle \mathbf{1}_{NS}, \mathbf{1}_{NS}^\top \rangle.$$

1541 Therefore,  $\Phi$  is bounded above by

$$\begin{aligned}
 \Phi &\leq \frac{\gamma}{NS} \langle [\partial_{f_{\theta^t}} \mathcal{L}(f_{\theta^t}; \mathbf{S}_i)]_N^\top, \mathbf{1}_{NS} \rangle \langle \mathbf{1}_{NS}^\top, [\partial_{f_{\theta^t}} \mathcal{L}(f_{\theta^t}; \mathbf{S}_i)]_N \rangle \\
 &= \frac{\gamma}{NS} \left( \sum_{i=1}^N \sum_{j=1}^S \partial_{f_{\theta^t}} \mathcal{L}(f_{\theta^t}; \mathbf{S}_{i(j,:)}) \right)^2.
 \end{aligned} \tag{48}$$

1548 Moreover, the last term in Equation 47 is also bounded above:

$$\begin{aligned}
 &\eta^2 \tau^2 \cdot [\partial_{f_{\theta^t}} \mathcal{L}(f_{\theta^t}; \mathbf{S}_i)]_N^\top \frac{\langle [K_{\mathbf{S}_i}]_N, [K_{\mathbf{S}_i}]_N^\top \rangle_{\mathcal{H}}}{NS} \cdot \bar{\mathbf{K}} \cdot \frac{\langle [K_{\mathbf{S}_i}]_N, [K_{\mathbf{S}_i}]_N^\top \rangle_{\mathcal{H}}}{NS} \cdot [\partial_{f_{\theta^t}} \mathcal{L}(f_{\theta^t}; \mathbf{S}_i)]_N \\
 &\leq \eta^2 \tau^2 \left[ \frac{\gamma}{NS} \sum_{i=1}^N \sum_{j=1}^S \partial_{f_{\theta^t}} \mathcal{L}(f_{\theta^t}; \mathbf{S}_{i(j,:)}) \right]^\top \cdot \bar{\mathbf{K}} \cdot \left[ \frac{\gamma}{NS} \sum_{i=1}^N \sum_{j=1}^S \partial_{f_{\theta^t}} \mathcal{L}(f_{\theta^t}; \mathbf{S}_{i(j,:)}) \right]_N \\
 &\leq \frac{\eta^2 \tau^2 \gamma^3}{NS} \left\langle \left[ \frac{1}{NS} \sum_{i=1}^N \sum_{j=1}^S \partial_{f_{\theta^t}} \mathcal{L}(f_{\theta^t}; \mathbf{S}_{i(j,:)}) \right]_N^\top, \mathbf{1}_{NS} \right\rangle \left\langle \mathbf{1}_{NS}^\top, \left[ \frac{1}{NS} \sum_{i=1}^N \sum_{j=1}^S \partial_{f_{\theta^t}} \mathcal{L}(f_{\theta^t}; \mathbf{S}_{i(j,:)}) \right]_N \right\rangle \\
 &= \frac{\eta^2 \tau^2 \gamma^3}{NS} \left( \sum_{i=1}^N \sum_{j=1}^S \partial_{f_{\theta^t}} \mathcal{L}(f_{\theta^t}; \mathbf{S}_{i(j,:)}) \right)^2.
 \end{aligned} \tag{49}$$

1562 Thus, by combining Equations 46, 47, 48, and 49, we get  
 1563

$$\Upsilon \leq -\eta \gamma \left( \frac{3}{4} - \eta^2 \tau^2 \gamma^2 \right) \left( \frac{1}{NS} \sum_{i=1}^N \sum_{j=1}^S \partial_{f_{\theta^t}} \mathcal{L}(f_{\theta^t}; \mathbf{S}_{i(j,:)}) \right)^2, \tag{50}$$

1566 which means

1567

1568 
$$\frac{\partial \mathcal{L}}{\partial t} \leq \Upsilon \leq -\eta\gamma \left( \frac{3}{4} - \eta^2\tau^2\gamma^2 \right) \left( \frac{1}{NS} \sum_{i=1}^N \sum_{j=1}^S \partial_{f_{\theta^t}} \mathcal{L}(f_{\theta^t}; \mathbf{S}_{i(j,:)}) \right)^2. \quad (51)$$
 1569  
1570

1571

1572 Hence, if  $\eta \leq \frac{1}{2\tau\gamma}$ , it follows that

1573

1574 
$$\frac{\partial \mathcal{L}}{\partial t} \leq -\frac{\eta\gamma}{2} \left( \frac{1}{NS} \sum_{i=1}^N \sum_{j=1}^S \partial_{f_{\theta^t}} \mathcal{L}(f_{\theta^t}; \mathbf{S}_{i(j,:)}) \right)^2 = -\frac{\eta\gamma}{2} \left( \frac{1}{NS} \sum_{i=1}^N \sum_{j=1}^S \frac{\partial \mathcal{L}(f_{\theta^t}(\mathbf{S}_i)_{(j,:)}, \mathbf{y}_{i(j,:)})}{\partial f_{\theta^t}(\mathbf{S}_i)_{(j,:)}} \right)^2. \quad (52)$$
 1575  
1576

1577 ■

1578

1579

1580

1581

1582

1583

1584

1585

1586

1587

1588

1589

1590

1591

1592

1593

1594

1595

1596

1597

1598

1599

1600

1601

1602

1603

1604

1605

1606

1607

1608

1609

1610

1611

1612

1613

1614

1615

1616

1617

1618

1619

1620 C EXPERIMENT DETAILS  
16211622 C.1 LLMs TRAINING SETTING  
1623

1624 All experiments were conducted on 4 NVIDIA A100 (80GB) GPUs. We employ LoRA fine-tuning  
1625 following the Alpaca (Taori et al., 2023) and Pizza (Meng et al., 2024) implementation strategy.  
1626 Specifically, we optimize with AdamW using a batch size of 128, a learning rate of  $2e-5$ , cosine  
1627 annealing scheduling (Loshchilov & Hutter, 2017), and a warmup ratio of 0.03, without weight decay.  
1628 The training objective computes loss only over responses from the selected datasets. We configure  
1629 LoRA with `lora_alpha=lora_r`, set `lora_dropout`, and insert adapters into all linear layers of the base  
1630 model. Both the backbone and adapters are trained in `Float32` precision.  
1631

1632 **AtteNT Setting** In this experiment, we adopt a straightforward variant of AtteNT: the model is  
1633 trained on the full dataset during the first epoch, after which only the AtteNT selected subset is used  
1634 in subsequent epochs. Selection is guided by the per-sample loss scores within each epoch, effectively  
1635 directing the model’s attention toward harder examples. Since pretrained models already perform  
1636 well on most instances, emphasizing more challenging data in later epochs is expected to yield greater  
1637 fine-tuning benefits. Following prior findings in Rho-1 (Lin et al., 2024), we set the selection ratio to  
1638 70%.

1639 **Dataset Building** The ImageNetS50 dataset is derived from the ImageNet-1k benchmark, and  
1640 its construction requires access to a local copy of ImageNet-1k. Following the official reposi-  
1641 tory (Gao et al., 2021), we generate ImageNetS50 by running `data_preparation.sh`  
1642 with the option `-mode=50`. Semantic segmentation annotations are obtained using  
1643 `datapreparation_anno.sh`. For depth annotations, we employ the Mask2Former (Cheng  
1644 et al., 2022) framework, utilizing its released code and pretrained models to generate pseudo-labels.  
1645 In addition, we directly download the full NYUv2 dataset, where the official semantic segmentation  
1646 and depth test sets are used for evaluation.  
1647

1648 C.2 ViTs TRAINING SETTING  
1649

1650 We adopt ViT-B (Dosovitskiy et al., 2020) with a  $16 \times 16$  patch size as the backbone for our MAE  
1651 experiments and evaluate performance on ImageNet-S50. Training is performed using AdamW with  
1652 a base learning rate of  $1e-4$  and weight decay of 0.05. The learning rate is linearly warmed up for 40  
1653 epochs, followed by cosine decay scheduling (Loshchilov & Hutter, 2017). We train with a batch size  
1654 of 2048 on 4 A100 GPUs, leveraging automatic mixed precision for efficiency. Data augmentation is  
1655 limited to standard transformations: random cropping with scale sampled from [0.2, 1.0] and aspect  
1656 ratio from [0.75, 1.33], resizing to  $224 \times 224$ , and random horizontal flipping with probability 0.5. A  
1657 full specification of hyperparameters for pretraining and fine-tuning is provided in Tables 5 and 6.  
1658

1659 Table 5: Hyperparameters for pre-training Multi-Modal MAE.  
1660

1661 <b>Hyperparam</b>	1662 <b>Baseline</b>	1663 <b>AtteNT</b>
1664 Batch Size	2048	2048
1665 Learning Rate	$1e-4$	$1e-4$
1666 Min Learning Rate	$1e-6$	$1e-6$
1667 Weight Decay	0.05	0.05
1668 Adamw $\epsilon$	$1e-8$	$1e-8$
1669 Adamw $\beta_1$	0.9	0.9
1670 Adamw $\beta_2$	0.95	0.95
1671 Epoch	800	800
1672 Warm up Epoch	40	40
1673 Learning Rate Schedule	cosine decay	cosine decay
Non-masked tokens	98	98
Input resolution	$224 \times 224$	$224 \times 224$
Augmentation	RandomResizeCrop	RandomResizeCrop
Dropout	0.0	0.0
Patch Size	16	16
Selection	{None}	{Random, Hard, Soft}

1674  
 1675 Table 6: Hyperparameters for fine-tuning Multi-Modal MAE on various downtasks. The augmentation  
 1676 strategy LSJ is large scale jittering (Ghiasi et al., 2021). We use drop path (Huang et al., 2016) in  
 1677 classification and semantic segmentation tasks.

Hyperparam	ImageNetS50	NYUv2(S)	NYUv2(D)
Epoch	100	100	2000
Warm up Epoch	5	20	100
Batch Size	1024	1024	2048
Learning Rate	4e-3	1e-4	1e-4
Min Learning Rate	1e-6	1e-6	0
Weight Decay	0.05	0.05	1e-4
Adamw $\beta_1$	0.9	0.9	0.9
Adamw $\beta_2$	0.999	0.999	0.999
Layer Decay	0.65	0.75	0.75
Patch Size	16	16	16
Drop path	0.1	0.1	/
LR Schedule	cosine decay	cosine decay	cosine decay
Input resolution	224×224	224×224	256×256
Augmentation	Rand(9, 0.5)	LSJ	LSJ

1691  
 1692 **AtteNT Setting** We employ an enhanced AtteNT strategy that dynamically selects training data  
 1693 based on per-sample loss scores. Specifically, data selection in the first epoch is guided by each  
 1694 sample’s initial loss, and the selection is periodically updated by recomputing loss scores after fixed  
 1695 intervals. This updated subset is then used to initiate the next training stage. Moreover, we incorporate  
 1696 a dynamic selection ratio from 20% to 80%, following the adaptive scheme proposed by (Zhang  
 1697 et al., 2023b). As demonstrated in Section 5, this approach achieves a favorable trade-off between  
 1698 efficiency and performance.

1699 **Dataset Building** All datasets used in our experiments are available on HuggingFace:

- 1702 • Mathematical Reasoning: Training on meta-math/MetaMathQA; evaluation on  
 1703 openai/gsm8k and hendrycks/MATH.
- 1704 • Code Generation: Training on m-a-p/CodeFeedback (restricted to Python samples);  
 1705 evaluation on openai/humaneval and google/mbpp.
- 1706 • Multi-Turn Dialogue: Training on WizardLM/evol\_instruct\_196k; evaluation on  
 1707 lmsys/mt-bench.

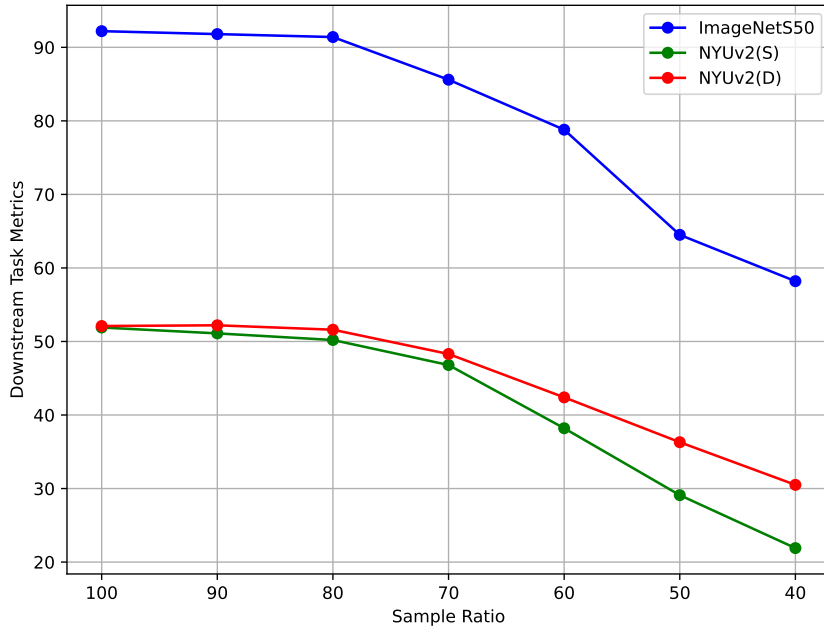
1708  
 1709  
 1710  
 1711  
 1712  
 1713  
 1714  
 1715  
 1716  
 1717  
 1718  
 1719  
 1720  
 1721  
 1722  
 1723  
 1724  
 1725  
 1726  
 1727

1728  
1729 D ADDITIONAL EXPERIMENTS

## 1730 D.1 ABLATION OF SAMPLE RATIO

1732 Table 7: Sample Ratio Study of ViT models.  
1733

Tasks \ Ratio	100	90	80	70	60	50	40
ImageNetS50	92.2	91.8	91.4	85.6	78.8	64.5	58.2
NYUv2(S)	51.9	51.1	50.2	46.8	38.2	29.1	21.9
NYUv2(D)	52.1	52.2	51.6	48.3	42.4	36.3	30.5

1762 Figure 4: Downstream Task Performance vs Sample Ratio.  
17631764 In this section, we investigate the impact of the AtteNT algorithm’s sample ratio on downstream  
1765 tasks. In Table 7, we compare the results based on the ViT model using different fixed sample ratios.  
17661767 As we can see from Fig 4, there is a noticeable drop in performance around the 80% selection  
1768 ratio. This suggests that, during training, a portion of the data remains relatively unchanged and  
1769 contributes less to performance when its selection ratio falls below a certain threshold (Lin et al.,  
1770 2024; Katharopoulos & Fleuret, 2018). When the ratio of unselected samples during training is lower  
1771 than this threshold, the model can maintain its performance. Interestingly, a small data drop can even  
1772 act as a form of noise reduction.

## 1773 D.2 COMPARISON TO ESTABLISHED METHODS

1776 Table 8: Performance Comparison of Different Methods.  
1777

Methods	Time( $\downarrow$ )	ImageNetS50( $\uparrow$ )	NYUv2(S)( $\uparrow$ )	NYUv2(D)( $\uparrow$ )
AtteNT(Ours)	980m	92.3	52.6	57.2
Class Weight Sampling	1108m	90.4	48.2	52.0
Fixed Weight Sampling	1065m	89.6	49.7	54.6
GradNorm Sampling (Chen et al., 2018)	1112m	91.9	52.4	55.8

As shown in Table 8, we also performed experiments comparing AtteNT with three simple yet representative sample-selection baselines to compare with traditional greedy algorithm: The first method, Class-Weight Sampling, assigns sampling weights inversely proportional to the number of samples per class, aiming to encourage the model to treat all classes more equally (sampling weight =  $1 / \text{class frequency}$ ). The second, Fixed-Weight Sampling, assigns fixed sampling ratios based on prior beliefs about task difficulty. In our setting, we consider the classification task easier than semantic segmentation and depth estimation, so we reduce the sampling rate for the RGB modality and set fixed sampling weights to 1 : 2 : 2 (RGB : SemSeg : Depth). The third method, GradNorm Sampling (Chen et al., 2018), dynamically adjusts the sampling weights for data groups (RGB, SemSeg, Depth) based on their gradient contributions during training. All methods were trained for 800 epochs, with the total sampling budget fixed at 70% for each baseline.

Across all comparisons, AtteNT consistently achieves higher efficiency and stronger predictive performance. These results indicate that AtteNT’s gains do not arise from generic greedy sampling heuristics, but from its principled nonparametric teaching mechanism, which adapts to model uncertainty and task interactions more effectively than existing selection strategies.

### D.3 VISUALIZING NTK ANALYSIS

To empirically confirm that the neural tangent kernel quickly stabilizes in real vision transformer training, we track the NTK on 10 fixed training points during an 800-epoch run of the Multi-Modal MAE backbone:

- Figure 5: Frobenius norm of the difference between the empirical NTK at epoch and the canonical kernel. The difference falls sharply within the first 50 epochs and stays near zero thereafter.
- Figure 6: Heatmaps of the  $10 \times 10$  NTK at selected checkpoints. A clear pattern is already visible at epoch 139, and from epoch 219 onward the heatmaps are virtually identical and remain unchanged through epoch 799.

These quantitative and qualitative results jointly show that the empirical NTK converges extremely rapidly (within 50–200 epochs) and remains close to the canonical kernel for the rest of training.

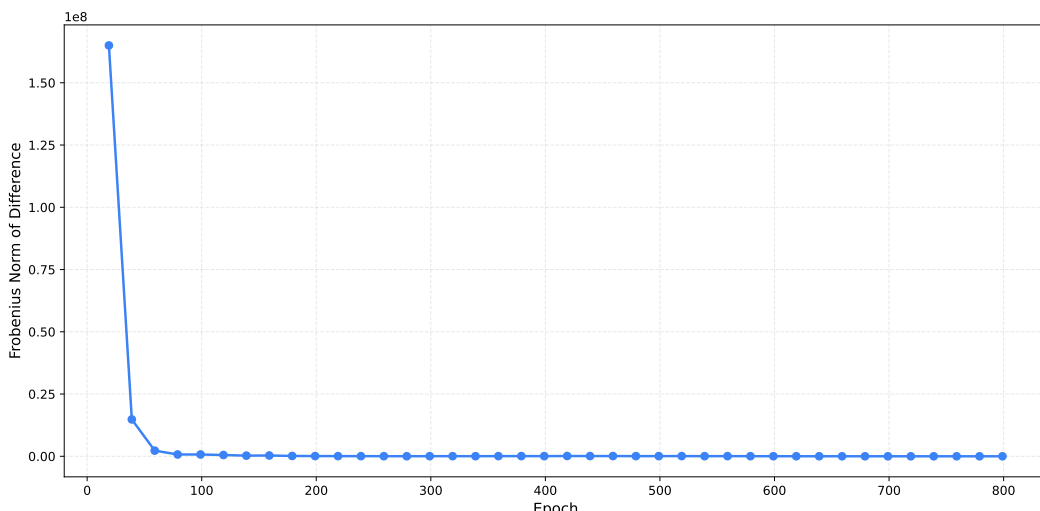


Figure 5: Frobenius norm of the difference between the empirical NTK at different training steps and the canonical kernel.

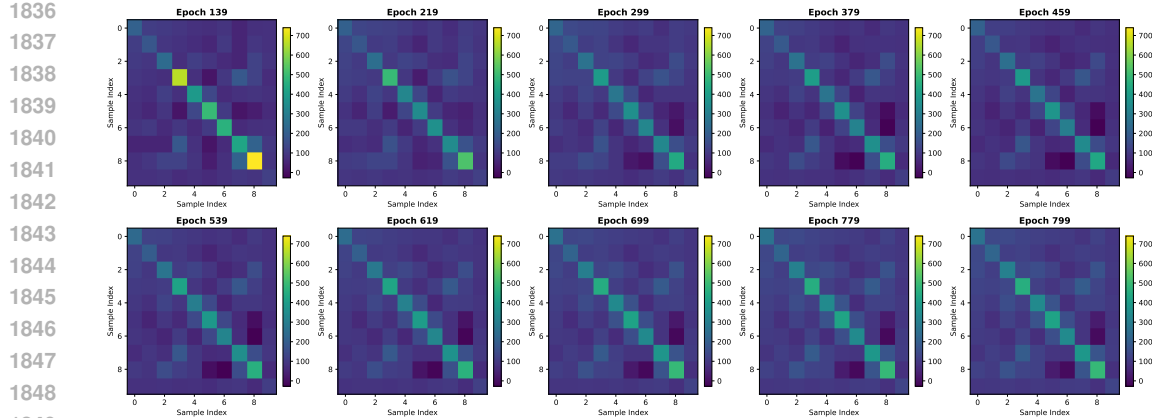


Figure 6: Evolution of the empirical  $10 \times 10$  NTK matrix during training. Color represents value  $K_{\theta^t}(S_i, S_j)$ . The matrix stabilizes visually after 200 epochs and shows negligible changes thereafter.

## E THE USE OF LARGE LANGUAGE MODELS (LLMs)

We used large language models for language polishing, such as grammar and phrasing. And we also use AI to assist with code completion. All research ideas, methods, analyses, figures, tables, and conclusions were solely developed by the authors. The authors take full responsibility for all content.

1859  
1860  
1861  
1862  
1863  
1864  
1865  
1866  
1867  
1868  
1869  
1870  
1871  
1872  
1873  
1874  
1875  
1876  
1877  
1878  
1879  
1880  
1881  
1882  
1883  
1884  
1885  
1886  
1887  
1888  
1889